



POLITECNICO

MILANO 1863

Reverse Engineering of Juno Mission Final report

Course of Space Systems Engineering & Operations
Academic Year 2023-2024

Group 5

Alex Cristian Turcu	alexchristian.turcu@mail.polimi.it	10711624
Chiara Poli	chiara3.poli@mail.polimi.it	10731504
Daniele Paternoster	daniele.paternoster@mail.polimi.it	10836125
Marcello Pareschi	marcello.pareschi@mail.polimi.it	10723712
Paolo Vanelli	paolo.vanelli@mail.polimi.it	10730510
Riccardo Vidari	riccardo.vidari@mail.polimi.it	10711828

Contents

Contents	i
Homework 1	1
Notation	1
1.1 Introduction	2
1.2 High level goals	2
1.3 Mission drivers	2
1.4 Functional analysis	3
1.5 Main mission phases	4
1.6 ConOps	4
1.7 Payload analysis	5
1.7.1 Instruments overview	5
1.7.2 Payload and Goals correlation	6
1.7.3 Payload and Phases/ConOps correlation	7
1.8 Mission analysis	7
1.8.1 Launch and cruise	7
1.8.2 Jupiter approach and insertion	7
1.8.3 Science operations and extended mission	8
1.8.4 Mission disposal	8
Bibliography	9
Homework 2	10
Notation	10
2.1 Mission analysis and ΔV budget	11
2.1.1 Rationale of the mission analysis	11
2.1.2 Simulation of the interplanetary trajectory	11
2.1.3 ΔV budget	12
2.2 Propulsion system architecture	13
2.2.1 Main Engine and RCS	13
2.2.2 Manoeuvre Implementation Modes	14
2.2.3 Tanks	15
2.3 Reverse engineering of propulsion system	15
2.3.1 Fuel and oxidizer tanks sizing	15
2.3.2 Pressurizer tanks sizing	16
2.3.3 Computation of actual propellants usage	17
Bibliography	18
Homework 3	19
Notation	19
3.1 TMTc system architecture	20
3.1.1 HGA	20
3.1.2 MGA & LGAs	21
3.1.3 TLGA	21
3.1.4 Ground stations	21
3.2 Phases breakdown	23
3.3 Reverse sizing of the HGA	23
Bibliography	25
Homework 4	26
Notation	26
4.1 Introduction of AOCS	27
4.2 Breakdown of Juno modes	27
4.2.1 Sun Pointing Mode (SPM)	27
4.2.2 Earth Pointing Mode (EPM)	27
4.2.3 GRAVity science Mode (GRAVM)	27

4.2.4	MicroWave Radiometer Mode (MWRM)	28
4.2.5	Turn-Burn-Turn Mode (TBTM)	28
4.2.6	VECtor Mode (VECM)	28
4.2.7	Spin Change Mode (SCM)	29
4.2.8	Safe Modes (SM)	29
4.2.9	Pointing budget & Phases/AOCS modes correlation	29
4.3	Architecture and rationale of AOCS	29
4.3.1	Sensors	30
4.3.2	Actuators	30
4.3.3	Rationale	31
4.4	Reverse sizing of AOCS	31
4.4.1	Modeling hypothesis	31
4.4.2	Perturbations	32
4.4.3	Propellant reverse sizing	33
4.5	Appendix	34
4.5.1	Simulink model description	34
	Bibliography	35
Homework 5		36
	Notation	36
5.1	Introduction of TCS	37
5.2	Analysis of thermal conditions along the mission	37
5.2.1	Thermal phases analysis	37
5.2.2	External heat flux analysis	37
5.3	Architecture and rationale of TCS	39
5.3.1	Vault	39
5.3.2	Main body	39
5.3.3	Solar panels	40
5.3.4	External hardware	40
5.4	Reverse sizing of TCS	41
5.4.1	Main body	41
5.4.2	Solar panels	42
5.5	Appendix	43
5.5.1	Thermal limits and power usage of instrumentation	43
	Bibliography	44

Homework 1

Notation

MAG	Magnetometer	JEDI	Jupiter Energetic-particle Detector Instrument
HGA	High Gain Antenna	JADE	Jovian Auroral Distribution Experiment
ΔV	Velocity budget	UVS	Ultraviolet Spectrograph
DSN	Deep Space Network	JIRAM	Juno Infra-Red Auroral Mapper
LEOP	Launch and early orbit phase	EGA	Earth Gravity Assist
SECO	Second engine cut off	JOI	Jupiter Orbit Insertion
L+	Time after launch	DSM	Deep Space Manoeuvre
PJ	Perijove number	PRM	Period Reduction Maneuver
MWR	Microwave Radiometer	GSO	Gravity Science Orbit

1.1 Introduction

Juno is a NASA spacecraft orbiting Jupiter. Built by Lockheed Martin and operated by NASA, it was launched by an Atlas V551 on the 5th of August 2011. After 5 years, during which many maneuvers occurred, including an Earth flyby, Juno entered a polar orbit around Jupiter and started its observation, which lasts to this day. Its aim is to study the planet to understand its composition and evolution, analyzing its gravitational and magnetic fields and its atmosphere dynamics. The mission should have ended in 2017, but it is still ongoing^[1] and it will end with a de-orbit that will destroy the spacecraft into the planet's atmosphere to avoid contaminating the environment.

1.2 High level goals

Through an analysis of the mission and payload, the main goals of the mission can be highlighted.

1. How did Jupiter form and influence the solar system?^{[2][3]}

Since Jupiter is the biggest planet of the solar system, it has influenced the formation of all other planets. Its composition has remained unchanged ever since, making it like a time capsule: understanding how and where it formed could give knowledge on Earth and the whole solar system's origin, evolution and characteristics.

2. What's Jupiter's deep structure?^{[3][4]}

One important aspect of the mission is the analysis of Jupiter's deep structure through the measurement of radiations, magnetic and gravitational fields. This allows to comprehend whether or not the planet has a solid nucleus, if so how large it is, and to analyze the supposed layer of metallic hydrogen, compressed so much that it loses its electrons creating a conducting layer. Moreover, Juno will possibly reveal if Jupiter is rotating as a solid body or if the rotating interior is made up of concentric cylinders.

3. What's the structure of Jupiter's atmosphere?^{[3][5]}

One of the mission's goals is to study the composition and dynamics of Jupiter's atmosphere, composed by stripes and dots made of different gasses and vapors, including water, whose percentage has to be defined. A significant aspect of the analysis is the great red spot, a swirling mass of gas bigger than Earth, which resembles a hurricane but is very different in the way it works. The movement of stripes and dots is dictated by the weather, characterized by lighting and thunderstorms, which are observed by Juno.

4. What do auroras look like and what are the physical processes generating them?^{[3][5]}

Juno's orbit is designed to be polar, to allow the observation of Jupiter's poles and the analysis of its auroras, representative of the interaction between charged particles and the atmosphere. Studying this phenomenon allows a better understanding of the atmospheric composition and the magnetic field's structure and extension.

5. What do the poles look like?^[3]

One of Juno's side goals is the observation of Jupiter's poles, which had never been possible before because of the absence of a polar orbiting spacecraft. This also increments the public's involvement in the mission.

1.3 Mission drivers

Being Juno an interplanetary mission starting from a distance of around 1 AU, with a final nominal distance from the Sun of 5.2 AU, and operating in a highly radiation intense environment, the following drivers have been identified:

1. Using proven technologies^[6]

The total program is financed with 1.1 Billion \$ for 74 months from the launch date and includes development of the spacecraft, science instruments, launch services, mission operations, science processing and relay support. The simplicity and the need of proven technologies was thus fundamental. The spacecraft is mainly maintained stable during the maneuvers thanks to its spin, raised to 5 RPM from 2, nominal condition during science operations, reducing the need of active stabilization methods.

2. Providing enough electricity during the duration of the mission^{[3][6][7][8][9]}

The journey of Juno is long and passes through different regions of the solar system. Solar panels were chosen to provide electric energy across the mission over a nuclear source, since it has been decided that it was better to advance technology of solar cells rather than developing a new reactor. It is the first spacecraft to operate with solar panels at such distance from the Sun. The system needed is thus oversized at 1 AU: the solar radiation on Jupiter is in fact up to 96% lower than on Earth. Furthermore the operations are scheduled to begin around 5 years into the mission, so degradation of the solar cells must be taken into account. The final design consists in 11 solar panels, eight are 9 by 2.65 m each, meanwhile the inner three are only 2 m wide, resulting in a surface of about 60 m² and granting a maximum power of 14 kW around Earth and up to 500 W around Jupiter. The solar panels are mounted in three arrays on the side of hexagonal body of the spacecraft at 120° one by the other, three arrays are composed by 4 panels, one by 3. This configuration is needed to mount the MAG faraway from the electronics and store everything correctly inside the fairing. Before separation from the upper stage, the spacecraft is spinning at around 1.4 RPM and the deployment of the solar arrays slows it down to 1 RPM. Moreover, since the fly-by around Earth is done to gain ΔV , the spacecraft will be in an eclipse for around 20

minutes: attention must be paid to size the battery. Two lithium-ions battery of 55 Ah each are present to make sure power is always provided. The nominal polar orbit around Jupiter allows Sun pointing during the majority of nominal Science Operation phase.

3. Shielding the instruments from the harsh environment of Jupiter^{[1][2][10][11]}

To accomplish its goals, Juno will need to cross the Jupiter radiation belts: a heavy shielding structure is needed. The magnetosphere represents a great challenge for Juno: the value of the magnetic field measured at its perijove is $776 \mu\text{T}$, 50% higher than expected. The main issue with Juno is represented by the ionizing particles present in the belt around Jupiter: with measured value up to of tens and hundreds of MeV ions located between 2 and $4 R_J$, order of GeV were expected under $2 R_J$, where Juno should pass through to reach a lower altitude, thanks to its highly elliptical orbit, where radiations are lower, to perform science. The vault in which all the electronics is preserved is cubed shaped and it is made of 1 cm thick titanium alloy, 144 kg in total. The top deck of Juno is planned to receive a radiation dose of 22 Mrad. Moreover, star trackers are also heavily shielded.

4. Maintaining communication during the journey and the science operations^[6]

The attitude of the spacecraft is defined in a way to point Earth during most of the cruise and science operations. This configuration, given the distance from the Sun and the Earth, grants also a sufficient inclinations of the solar panels with respect to the Sun to provide enough electric power. The ground equipment used by Juno is NASA's DSN.

1.4 Functional analysis

Functional analysis is performed in order to identify the functionalities that the spacecraft must perform during the mission. The identified functionalities are schematized in Figure 1.1.



Figure 1.1: Functional analysis for Juno mission

1.5 Main mission phases

The Juno mission was divided into five phases: LEOP, Cruise, Jupiter approach and insertion, Science Operations and De-orbit.

1. LEOP

Following the launch from Cape Canaveral, the spacecraft entered a low Earth parking orbit.^[6] Afterwards Juno was injected in an interplanetary trajectory and was separated from its upper stage after SECO-2 at time L+54 min. The solar panels deployment was performed about five minutes after the spacecraft separation, and it took approximately five minutes.

2. Cruise

The cruise had a duration of about five years, during which two deep space manoeuvres, multiple minor corrections and an Earth fly-by were performed. All manoeuvres will be better described in [section 1.8](#). This phase also included instruments testing and verification, to ensure they were functioning properly and ready for the usage during the mission.

3. Jupiter approach and insertion

This phase began four days before the start of orbit insertion manoeuvre and ended one hour after the start of the orbit insertion manoeuvre. The latter occurred at closest approach to Jupiter and slowed the spacecraft down enough to let it be captured by Jupiter in a 53-days period orbit. The Jupiter orbit insertion burn was performed by the Leros 1-b main engine, and it lasted 30 minutes. After the burn, the spacecraft was in a polar orbit around Jupiter. The 53-days orbit provided substantial propellant savings with respect to the direct insertion in the operational orbit.

4. Science operations

The Juno polar and highly eccentric orbit was designed to facilitate the close-in measurements and to minimize the time spent in the Jupiter radiation belts. During this phase all the science operations, in different attitudes, are being performed.

5. De-orbit

The de-orbit phase will occur during the final orbit of the mission. The latter was designed to satisfy NASA's planetary protection requirements and ensure that Juno doesn't impact any of Jupiter's moons. A de-orbit burn will be performed, placing the spacecraft on a trajectory towards Jupiter inner and denser layer of the atmosphere where it will burn up.

1.6 ConOps

The mission's Conceptual Operations are summarized in [Figure 1.2](#).



Figure 1.2: Conceptual Operations, time not in scale^{[2][6][12][13]}

1.7 Payload analysis

1.7.1 Instruments overview

As previously described in section 1.2 the mission scientific goals are quite numerous and diverse. Thus, to achieve all of them, the payload consists of several instruments, nine to be precise, covering a wide spectrum of experimentation. In its entirety the payload has a mass of around 174 kg and consumes approximately 125 W of power excluding the Gravity science experiment.^[7] Here we have a brief overview of all the singular instruments where, unless otherwise specified, only the sensors are mounted on the exterior of the spacecraft, while all the relevant electronics are located inside the radiation vault.

- **Magnetometer (MAG):** As the name implies its objective is to accurately measure Jupiter's magnetic field, achieved by employing two flux-gate magnetometers, a scalar helium magnetometer and two star cameras. All the sensors are mounted on the magnetometer boom, located at the end of one of the solar array wings to reduce the interference from the spacecraft itself. Even then the presence of two magnetometers allows to subtract this contribution from the measurement.
- **Microwave Radiometer (MWR):** It consists of six antennas which measure six different frequencies (600 MHz, 1.2 GHz, 2.4 GHz, 4.8 GHz, 9.6 GHz and 22 GHz) in order to investigate the Jovian atmosphere below the visible external layer. A key objective of this analysis is also the determination of the abundance of water inside the planet. The antennas are mounted on two sides of the hexagonal prism that constitutes the main body of the spacecraft, relying on its spin to survey Jupiter.
- **Gravity science:** It's quite a unique instrument as it's composed both by a space and a ground elements, which mainly consists with the telecommunication systems of both the spacecraft and ground stations. This is because this experiment is based on measuring the doppler shift in the returning signal from Juno which, allows to characterize Jupiter's gravitational field. Thus the instrument can't really be separated from the telecommunication hardware, which is the reason why its weight and power requirement were omitted in the previously shown totals.
- **Jupiter Energetic-particle Detector Instrument (JEDI):** It detects high energy electrons and ions present in the Jovian magnetosphere, which are discriminated by composition. Each sensor is characterized by six electron and six ion viewing directions that together cover a $160^\circ \times 12^\circ$ field of view. In total three sensors are present on Juno, two arranged to obtain an almost complete 360° view perpendicular to the spacecraft spin axis, while the third one is instead aligned with it to achieve a full scan of the sky over one spin period. As the JEDI sensors are self-contained units no electronic hardware is present within the radiation vault.
- **Jovian Auroral Distribution Experiment (JADE):** It detects low energy electrons and ions with the same goal of characterizing the magnetosphere as JEDI. The instrument comprises of three identical electron energy per charge analyzers (JADE-E) and a single ion mass spectrometer (JADE-I). The electron sensors are located on the three sides of the spacecraft that do not house the solar arrays pointing outwards, to again obtain a complete view normal to the spin axis. The spectrometer field of view, instead, contains the spin axis and like the third JEDI sensor it scans all the sky over a full rotation.
- **Ultraviolet Spectrograph (UVS):** This instrument images and measures the spectrum of the Jovian aurora in order to understand its morphology and source. The chosen ultraviolet range of $68 \div 210$ nm covers all of the most important UV emissions from the aurora, mainly the H Lyman series and longer wavelengths from hydrocarbons. The sensor is mounted on the side of Juno, relying once more on the spinning of the spacecraft to achieve a full sweep of the planet.
- **Radio and Plasma Waves (Waves):** Its objective is to study both components of the electromagnetic field generated by plasma and radio waves inside the polar regions of Jupiter's magnetosphere to understand its interaction with the atmosphere and magnetic field. To detect the electric component a V-shaped dipole antenna is used, while for the magnetic component a much smaller magnetic search coil is employed. Both sensors cover a vast range of frequencies, namely from 50 Hz up to 40 MHz.
- **Visible-spectrum Camera (JunoCam):** It's designed to provide highly detailed color images of Jupiter to help and support public engagement of the mission without any real scientific purpose. The instrument is thus only comprised of the camera itself, mounted on the side of the spacecraft, and all the necessary electronics which, given the less critical objective and relaxed radiation tolerance requirements, aren't housed in the radiation vault.
- **Juno Infra-Red Auroral Mapper (JIRAM):** It's an infrared imager and spectrometer that studies the Jovian atmosphere in the $2 \div 5 \mu\text{m}$ range complementing both the atmospheric and magnetospheric experiments. This instrument is also completely housed outside of the radiation vault since it is a late addition after mission selection, reason for both the relaxed radiation requirements and less than ideal positioning of the sensor on the aft deck of the spacecraft.

All the instruments and their positions can be seen in Figure 1.3.



Figure 1.3: Positioning of the instruments on the spacecraft

1.7.2 Payload and Goals correlation

There is a notable overlap in the main objectives of the payload instruments, both in the sense that multiple ones collaborate towards a single scientific goal, but also in the sense that a single instrument can address multiple goals. All of these relations are exemplified in Table 1.1.

Guiding questions	Science objectives	Measurements objectives
How did Jupiter form and influence the solar system?	Determine Jupiter's inner composition	Composition analysis: MWR
What's Jupiter's deep structure?	Analyze gravitational and magnetic field, measure water abundance in the planet	Gravitational field analysis: Gravity science Magnetic field analysis: MAG Water abundance measurements: MWR
What's the structure of Jupiter's atmosphere?	Analyze atmospheric composition and dynamics	Atmospheric composition determination: MWR Atmospheric dynamics study: JIRAM
What do auroras look like and what are the physical processes generating them?	Image auroras, study interactions between atmosphere and magnetic field, characterize the magnetosphere in the polar regions	Imaging auroras: UVS, JIRAM Atmosphere-magnetic field interaction: JIRAM Characterize the magnetosphere: Waves, JADE, JEDI

Table 1.1: Mission goals and instrument objectives correlation

It can be noted that the JunoCam instrument doesn't appear in the table since it's not part of the scientific goals of the mission, as previously mentioned in its description.

1.7.3 Payload and Phases/ConOps correlation

Another high-level correlation can be highlighted between the mission phases/ConOps and the activities of the payload as shown in Table 1.2.^[6]

Mission phases	Payload activities
LEOP	Mag boom is deployed together with solar arrays
Cruise	Instruments checks are performed regularly and the high gain antenna (used for Gravity science) is calibrated and aligned
Jupiter approach and insertion	Final instruments checks are carried out together with some initial scientific observations of Jupiter
Science operations	Complete nominal operation of the payload with observations divided between Gravity science passes (Earth pointing) and MWR passes (Nadir pointing)
De-orbit	No planned payload operations

Table 1.2: Mission phases/ConOps and Payload activities correlation

1.8 Mission analysis

1.8.1 Launch and cruise

The spacecraft was launched into orbit with an Atlas V 551 Rocket from Cape Canaveral. The actual launch date belonged to a 21-day time window limited by a number of events and their timings such as the Deep Space Maneuvers, the Earth Flyby, the Jupiter Insertion and the science orbits. The adopted transfer strategy allowed for significant reduction in ΔV with respect to a direct transfer between Earth and Jupiter.

Following the launch, after booster separation, Juno was put in a low Earth parking orbit thanks to a first burn of the Centaur upper stage. Afterwards, at time L+645 s, via a second burn given by the same stage, Juno entered an heliocentric trajectory. Solar arrays were deployed and initial checks on the instruments were performed at this time. This procedure is fundamental in order to provide enough electrical power to the spacecraft to perform initial check on its health. The specific trajectory followed by Juno is called "2 + dV-EGA", which means that the spacecraft will perform an Earth gravity assist at around two years after launch. During the initial cruise various correction maneuvers were performed: the main ones being the two DSMs needed to place Juno on the correct path to achieve the planned fly-by. DSMs were performed near the apocentre, located farther away from the Sun than Mars' orbit, causing the spacecraft to pass as close as 0.88 AU before approaching Earth. During the approach to perform the fly-by, attitude corrections were performed to protect the spacecraft by the incoming radiation from the Sun. The fly-by around Earth occurred on the 10th of September 2013 and puts the spacecraft on its final trajectory to Jupiter. Particularly, the fly-by gave the spacecraft 7.3 km/s, avoiding a fire-up of the Leros 1-b main engine of Juno. A last correction maneuver was performed to refine Juno's trajectory.^{[4][6][9][14][15]}



Figure 1.4: Juno's trajectory from ecliptic north pole

1.8.2 Jupiter approach and insertion

After the flyby, Juno spent 791 days on its last interplanetary leg in which no significant manuevers nor scientific operations were conducted. Jupiter approach lasted a further 178 days, during which calibration, validation of the on board instruments and telecommunications checks were accomplished. Initial science observations of Jupiter's distant environment were also performed.

JOI burn was made at the closest approach to Jupiter: this moment is called PJ-0, indicating the first passage at the perijove of Juno. The targeted point for this maneuver is at an altitude of 4200 km, calculated above the 1-bar level of Jupiter. The spacecraft is left on a highly elliptical 53-days period around Jupiter with an inclination of 90° ($\pm 10^\circ$). Additional clean-up manuevers were planned to correct the trajectory. The attitude during JOI phase, as the

spacecraft was slowing down, was such that the HGA was not pointing Earth, constraining communications to low tones, only meant to send information about the completion or failure of the events. After 50 hours from PJ0 all instruments were successfully powered up and started to perform nominal science operations.

1.8.3 Science operations and extended mission

The nominal science orbit, with a period of 14-days, had to be achieved via a PRM at PJ-02. This orbit had been chosen for many reasons:

- it allowed to avoid Jupiter's strongest radiation belts
- enabled near Sun pointing to generate enough electrical power and granted Earth communications via HGA
- it provided the closest possible approach of the instruments to Jupiter's clouds
- it allowed, thanks to Jupiter's oblateness, to scan the whole planet with only 32 orbits obtaining a resolution of 11.25°.

During science operations, two types of orbits should have been performed, differing in terms of spacecraft orientation: MWR passes, which required nadir pointing of Juno's spin plane in order to let the radiometers scan directly the planet, and GSOs, designed to align HGA with Earth.

However, due to a malfunctioning of an helium tank valve, Juno entered Safe Mode for 13.5 hours and PRW was discarded. This change showed the robustness of the designed capture orbit. It was in fact possible to conduct science operations on this longer path with only minor changes: the disposal of the spacecraft had to be moved from 2017 to 2021 to allow the completion of the 35 orbits. Moreover, the 53-days orbit required a slight plane change (from 90° to 105°) between PJ-22 and PJ-23 to avoid a solar eclipse since the batteries are only suited for the 19 minutes eclipse during the Earth fly-by.

The so conducted mission was scheduled to end on July 2021 but the conditions of the spacecraft and the remaining fuel on board allowed to extend the mission by other 42 orbits for 5 more years of mission. During the nominal phases, the PJ had been shifted northwards, so during the extended phase a series of close passes of Jupiter's north polar cyclones occurred. Furthermore, flybys of Ganymede, Io and Europa are performed in addition to an analysis of the faint rings of the observed planet.^[1]



Figure 1.5: Orbit around Jupiter

1.8.4 Mission disposal

Under the planetary protection requirements, Juno is designed to de-orbit itself after the extended mission succeeds. The dose of radiations absorbed during the lifetime of the spacecraft won't allow for safe operations. The de-orbit maneuver is supposed to begin with an apocentre burn, slowing down Juno by 75 m/s, enough to lower its perijove in the atmosphere of Jupiter. The dense gas layers will cause the spacecraft to disintegrate.

De-orbiting the spacecraft, now planned in 2025, will eliminate the possibility of contamination of Jupiter and its Moons' environment, especially to avoid unreliable results from the planned ESA Juice mission, expected to enter Jupiter's orbit in 2031.^{[12][13]}

Bibliography

- [1] Jet Propulsion Laboratory. *Juno Mission to Jupiter*. Site: <https://www.nasa.gov/>. 2022.
- [2] Richard Grammier. *Overview of the Juno Mission to Jupiter*. Site: <https://www.jpl.nasa.gov/missions/juno>. 2006.
- [3] Various. *Mission Juno - Great documentary on Jupiter and NASA's Juno probe*. Website. Site: <https://www.youtube.com/watch?v=ka60ERznXh4>. 2013.
- [4] Richard Grammier. "An overview of the Juno mission Jupiter". In: (2006).
- [5] S.J. Bolton J. Lunine D. Stevenson J.E.P. Connerney S. Levin T.C. Owen F. Bagenal D. Gautier A.P. Ingersoll G.S. Orton T. Guillot W. Hubbard. J. Bloxham A. Coradini S.K. Stephen P. Mokashi R. Thorne R. Thorpe. "The Juno mission". In: (2015).
- [6] *Advanced Global Optimisation Tools for Mission Analysis and Design*. NASA press kit. Site: https://www.jpl.nasa.gov/news/press_kits/JunoLaunch.pdf. 2011.
- [7] Chuck E. Rasbach Randy Dodge Mark A. Boyles. "Key and Driving Requirements for the Juno Payload Suite of Instruments". In: (2012).
- [8] Stephen F Dawson Paul Stella William McAlpine Brian Smith. *Juno Photovoltaic Power at Jupiter*. Site: <https://ntrs.nasa.gov/citations/20130010565>. 2012.
- [9] Various. *Spacecraft Information*. Website. Site: <https://spaceflight101.com/juno/spacecraft-information/>. 2024.
- [10] Installing Juno's radiation vault. *Radiation vault characteristics*. Website. Site: <https://www.nasa.gov/image-article/installing-junos-radiation-vault/>. 2024.
- [11] Connerney et al. *A New Model of Jupiter's Magnetic Field from Juno's First Nine Orbits*. Journal of Geophysical Research: Planet. Site: <https://agupubs.onlinelibrary.wiley.com/doi/10.1002/2018GL077312>. 2018.
- [12] NASA Jet Propulsion Laboratory. *NASA online press kit*. Website. Site: https://www.jpl.nasa.gov/news/press_kits/juno/. 2024.
- [13] NASA Jet Propulsion Laboratory. *NASA's Juno Mission Expands Into the Future*. Website. Site: <https://www.jpl.nasa.gov/news/nasas-juno-mission-expands-into-the-future>. 2024.
- [14] Various. *Juno Mission and Trajectory Design*. Website. Site: <https://spaceflight101.com/juno/juno-mission-trajectory-design/>. 2024.
- [15] NASA Horizons. *Ephemerides Data*. Website. Site: <https://ssd.jpl.nasa.gov/horizons/>. 2024.

Homework 2

Notation

ME	Main Engine	e_{cap}	Eccentricity of capture orbit [-]
RCS	Reaction Control System	NTO	Nitrogen Tetroxide
DSM	Deep Space Manoeuvre	O/F	Oxidizer to Fuel ratio
DSN	Deep Space Network	M_{dry}	Total dry mass of satellite [kg]
OTM	Orbit Trim Manoeuvre	M_{launch}	Total mass of satellite at launch [kg]
TCM	Trajectory Correction Manoeuvre	M	Total mass of satellite [kg]
SK	Station Keeping	M_p	Total mass of propellants [kg]
PRM	Period Reduction Manoeuvre	M_f	Total mass of fuel [kg]
JOI	Jupiter Orbit Insertion	M_{ox}	Total mass of oxidizer [kg]
REM	Rocket Engine Module	M_{He}	Total mass of helium [kg]
MEF	Main Engine Flush	V_{He}	Total volume of helium [m^3]
TRL	Technology Readiness Level	I_s	Specific impulse [s]
RW	Reaction Wheel	g_0	Standard gravitational acceleration [m/s^2]
COM	Centre Of Mass	r_{tank}	Radius of spherical propellants tanks [m]
MAG	Magnetometer	p_{tank}	Pressure of propellants tanks [Pa]
PC	Plane Change	T_{tank}	Temperature of propellants tanks [K]
ELA	Earth Look Angle	t_{tank}	Thickness of propellants tanks [m]
EGA	Earth Gravity Assist	V_{tank}	Volume of one empty propellants tank [m^3]
FB	Fly-by	M_{tank}	Mass of one empty propellants tank [kg]
INJ_J	Jupiter injection	$r_{tank,He}$	Radius of cylindrical helium tanks [m]
ESC_E	Earth escape	$h_{tank,He}$	Height of cylindrical helium tanks [m]
TLGA	Toroidal Low Gain Antenna	$t_{tank,He}$	Thickness of helium tanks [m]
HGA	High Gain Antenna	$M_{tank,He}$	Mass of one empty helium tank [kg]
SEP	Sun-Earth-Probe	R_{He}	Specific gas constant for helium [J/kg·K]
PED	Propellant Expulsion Device	γ_{He}	Adiabatic index for helium [-]
τ	Burn time [s]	Ti6Al4V	Titanium alloy
ΔV	Velocity change [m/s]	Al7075	Aluminum alloy
v_∞	Asymptotic velocity [m/s]	ρ	Density of the material [kg/m^3]
μ_J	Jupiter planetary constant [km^3/s^2]	σ	Tensile yield strength of the material [Pa]
r_p	Radius of pericentre [km]		

2.1 Mission analysis and ΔV budget

2.1.1 Rationale of the mission analysis

The mission analysis previously described could be split into two macro-phases:

- from launch to the interplanetary transfer, including DSMs and the Earth fly-by;
- planetary phase around Jupiter.

The main objectives of the mission analysis were to keep the overall launch energy C_3 and deterministic ΔV as low as possible, compliant with the constraints imposed by the navigation and spacecraft operational requirements. Regarding the interplanetary transfer, two main options were available, both including an EGA. The first option, named as "2 - dV EGA", contemplated a launch window time frame in October-November 2011. However, the latter was discarded since the approach angle at Jupiter would have resulted in a latitude farther away from the equator. This would have brought to higher radiation levels, hence a reduced time available for the science operations^[1]. The second option, named as "2 + dV EGA", contemplated a launch window time frame in August 2011 and it ended up being the chosen one. A viable back-up for this transfer would have happened in October 2012, since the basic features of "2 + dV EGA" repeat every 13 months. Regarding the interplanetary trajectory constraints, they could be divided into three categories:

- **Launch energy C_3 and timing constraints.** Fixing an initial value for the energy provided by the launcher, different possibilities of departure date could be analyzed. Every launch date defined a trajectory that was characterized by a required C_3 and deterministic ΔV . The maximum $C_3 = 31.1 \text{ km}^2/\text{s}^2$ was defined by the Atlas V551 launcher^[2]. Analyzing Juno's ephemeris for the actual launch date, the calculated value is $C_3 = 31.08 \text{ km}^2/\text{s}^2$. The trajectory reconstructed through the optimization problem and explained in subsection 2.1.2, revealed a value of $C_3 = 29.34 \text{ km}^2/\text{s}^2$, with departure date on 18th August 2011. Restricting the launch window domain around 5th August 2011 (the actual one) the value is $C_3 = 30.40 \text{ km}^2/\text{s}^2$. In the non-restricted window for departure, the trend of the C_3 over time can be evaluated in the work of Kowalkowski and Lam^[1].
- **Interplanetary events.** The milestones of this phase were DSMs and EGA. The fly-by was constrained to happen at a fixed altitude of 800 km well above ISS, but it could be lowered up to 500 km. This last decrease of the altitude value could have improved the robustness of the trajectory in the case of eventual delays in DSMs, decreasing also the ΔV of the mission and the intensity of the radiation at Jupiter arrival^[3]. However, the most challenging task was the selection of the DSM dates, in fact this choice would have affected the required launch C_3 and overall mission ΔV ^[1]. Moreover, DSM had to be split into two equally lasting burns, separated by two days. This was dictated by engine capabilities, described in subsection 2.2.1. As precaution, due to anomalous pressure and temperature values of the oxidizer feeding line during DSM-1, the two manoeuvres ended up being performed two weeks apart. An additional problem arose from the 2 + dV EGA interplanetary structure and the needs to perform the DSM at aphelion while having real-time visibility. This constraint was set up by imposing a SEP angle greater than 10° for acquisition of data, and SEP angle greater than 3° for execution of the manoeuvre. This difference was due to the need of seven days to plan the manoeuvre on ground after the necessary two days of data collection. In the eventuality of a burn before solar conjunction, an adequate time to retry failed attempts was considered. Another constraint regarding telecommunications and navigation was due to the positioning of the toroidal antenna (TLGA) which is used for ground link in the early phases and is mounted on the aft deck and aligned with the -Z-axis, as shown in Figure 2.2. To ensure a good signal with this antenna, the ELA was constrained to be within $\pm 10^\circ$ around 90°: since Doppler data is of very little value when ELA is too close to 90°, the combined range for the ELA resulted to be of 80° ÷ 87° and 93° ÷ 100°.
- **Jupiter arrival timing and geometry.** Jupiter arrival and insertion was constrained by multiple aspects. First of all, since a direct injection into the science orbit would have been too expensive, the burn was split into two manoeuvres (JOI and PRM), saving over 170 m/s^[1] related to gravity losses. In order to avoid longitudes at which the magnetic field is stronger, JOI and PRM dates had to be accurately selected. In addition, due to the critical nature of JOI, the manoeuvre had to take place during the overlapping coverage of two DSN complexes. Since the longest one was provided by Goldstone-Canberra, the burn and pre-burn events had to happen during that time frame. As far as PRM was concerned, dual DSN coverage was not required. However, the optimal date for PRM could be selected in order to minimize the overall ΔV and to manoeuvre at lower magnetic field longitudes. Lastly, the perijove was bounded to be at distances higher than 4500 km over the 1 bar pressure level of the atmosphere, allowing to operate in the hole of the torus that describes the highest radiation levels.

2.1.2 Simulation of the interplanetary trajectory

To reconstruct the interplanetary phase, a simulation was set up in *Matlab*. The implemented model considered three heliocentric legs, linked with the patched-conics method:

- from Earth to DSM position;

- from DSM position to fly-by at Earth;
- from fly-by position to Jupiter.

In order to minimize the total ΔV of the mission, a cost function was defined. This is determined by the sum of four contributions:

- $\Delta V_{esc,E}$: escape from Earth heliocentric orbit into the first interplanetary leg;
- ΔV_{dsm} : deep space manoeuvre;
- ΔV_{fb} : burn manoeuvre at Earth's fly-by hyperbola pericentre;
- $\Delta V_{inj,J}$: injection into Jupiter's heliocentric orbit.

The calculations were based on analytical ephemeris for the planets and the Lambert method was used to design the paths. The implementation was constrained by various inputs, according to the development of the mission:

- Earth departure date, defined in the interval from 05/08/2011 to 26/08/2011
- DSMs condensed in one impulsive burn
- DSM date, from 20/08/2012 to 10/09/2012
- DSM position domain constrained by means of keplerian parameters from the real mission ephemeris
- Fly-by date, from 20/09/2013 to 20/10/2013
- Fly-by altitude, of at least 500 km
- Jupiter arrival date, from 20/06/2016 to 10/07/2016

Then a genetic algorithm was used to minimize the cost function and the match between the calculations and Juno ephemeris was verified as shown in [Figure 2.1](#).



	ΔV [km/s]	Date
ESC_E	5.3920	14/08/2011
DSM	0.7225	29/08/2012
FB	$1.9872 \cdot 10^{-7}$	08/10/2013
INJ_J	5.4552	09/07/2016

[Table 2.1](#): Calculated solution

[Figure 2.1](#): Comparison of trajectories

The obtained results are coherent with the actual mission data^[4]. Regarding [Table 2.1](#), some values might seem particularly high in relation to the main engine capabilities. Indeed, not all of the ΔV s had to be performed by the main engine:

- $\Delta V_{esc,E}$ was executed by the upper stage of the Atlas V551, in the limits of the launcher performance C_3 .
- $\Delta V_{inj,J}$ was due to the rendezvous at Jupiter. The only burn required to enter an elliptical orbit had to be given at the pericentre of the hyperbola. The impulsive ΔV can be calculated as follows, considering $e_{cap} = 0.9884$ and $r_p = 75237.6$ km in relation to the designed 107 days orbit:

$$\Delta V_{JOI} = v_\infty \left(\sqrt{1 + \frac{2\mu_J}{r_p v_\infty^2}} - \sqrt{\frac{\mu_J(1 + e_{cap})}{r_p v_\infty^2}} \right) = 424.07 \text{ m/s} \quad (2.1)$$

Moreover, the low ΔV_{fb} value in [Table 2.1](#) indicates that gravity assist was not powered. Clean-up manoeuvre and TCMs were performed before and after the fly-by, hence this small burn.

2.1.3 ΔV budget

A summary of the planned, performed and simulated manoeuvres is exposed in [Table 2.2](#). The design column is referred to the pre-launch schedule, while the performed column is relative to the actual mission. The designed mission never saw life since various problems occurred during the cruise phase: from a nominal capture orbit with a period of 107 days and a science orbit of 11 days, the new scheduled orbits were of 53.5 days and 14 days respectively.

For this precise reason the performed values differ from the design ones, especially the JOI, which was related to a different capture orbit, and the PC, which was not meant to be performed originally. The whole simulation has been performed on the designed 107 days orbit and the 11 days one. The final two columns show the required ME burn times for the designed and the performed mission respectively.

Manoeuvres	Design [m/s]	Perf. [m/s]	Sim. [m/s]	τ_{ME} Design [min]	τ_{ME} Perf. [min]
TCM-1 ÷ 2 (RCS) ^[5]	4.4	1.71	-	-	-
DSM-1 (ME) ^[5]	360.1	344.16	722.51	30.97	29.71
DSM-2 (ME) ^[5]	394.8	387.94		30.07	29.77
TCM-4 ÷ 15 (RCS) ^[5]	32.5	7.89	-	-	-
MEF (ME) ^[5]	3.3	3.3	-	-	-
JOI (ME) ^[6]	424.07 ^I	541.73	424.07	27.86	35.65
JOI clean-up (RCS) ^[6]	4.92	6.39	-	-	-
PRM (ME) ^[6]	636	-	602.45	35.19	-
OTM pre-PC (RCS) ^[7]	120 ^{II}	94.88	-	-	-
PC (RCS)	-	56.39	69.97 ^{III}	-	-
OTM post-PC (RCS)	-	108.08	-	-	-
De-Orbit (RCS) ^[8]	75 ^{IV}	30.89 ^V	87.93	-	-

Table 2.2: Overall mission budget and simulation

^I This value has been assumed equal to the one calculated from the insertion on the 107 days orbit.

^{II} This value assumes 30 nominal science orbits with a required ΔV of 4 m/s.

^{III} This value is referred to the plane change of the 53 days orbit as no other trajectories required this manoeuvre.

^{IV} This value is assumed equal between the 11 days orbit and the 14 days orbit.

^V This value has been updated from the nominal 75 m/s since the de-orbit manoeuvre will be performed from a 53 days orbit and not from a 14 days orbit.

2.2 Propulsion system architecture

The spacecraft axes are defined as shown in Figure 2.2: the spacecraft is spinning along the +Z-axis, aligned with the HGA. The +X-axis is aligned with the MAG boom while the +Y-axis is in the direction of cross product between +Z-axis and +X-axis.



Figure 2.2: Axis description

2.2.1 Main Engine and RCS

Juno is equipped with a dual-mode propulsion system: the bi-propellant ME uses the hypergolic couple hydrazine and nitrogen tetroxide ($N_2H_4-N_2O_4$) while RCS uses hydrazine as monopropellant. This choice was made to simplify the design: fewer tanks are needed as fuel ones are shared between the two systems. Moreover, the choice of this specific hypergolic couple is dictated by the storage requirements of the mission: in a five-year cruise, reliability and sturdiness of the propulsive system were among the main drivers of the mission. Electric thrusters were discarded as TRL-9 technologies were required: other limitations such as power budget, an highly radioactive environment, weight and space inside the spacecraft required a more simple and light solution.

The ME is a Leros 1b, built by Nammo^[9], which produces about 662 N of thrust with $I_{s,me} = 318.6$ s. This particular engine is certified for a 42 minutes continuous burn and has a cumulative lifetime of 342 minutes, so the manoeuvres shown in Table 2.2 are compliant with this constraint. This engine is utilized during the DSMs, JOI and PRM. It is mounted inside the body of the spacecraft along the -Z-axis, centred between the propellant tanks and under the electronic vault. This solution has probably been adopted due to space requirements inside the Atlas V fairing and safety precautions during the cruise phase. The ME is also shielded by a hatch that opens when a manoeuvre is needed. The RCS is used for TCMs, attitude control and general SK. The catalyst used to decompose the hydrazine is the S-405, based on iridium and aluminum^[10]. The whole RCS is composed by four REMs, each of them mounted along the $\pm Y$ -axis on a pylon, as shown in Figure 2.3. Every pylon houses three thrusters, the MR-111C by Aerojet Rocketdyne^[11], pointed in different directions, each providing a thrust of 4.5 N with $I_{s,rcs} = 220$ s. Electrical power is required to operate the feeding valves, heating valves and the catalytic bed, amounting to a maximum of around 13 W^[12].



Figure 2.3: Forward and Aft deck view

The pylons are raised respectively by 74 cm on the forward deck and about 26 cm on the aft deck as shown in Figure 2.4. With the need of limiting even more the interaction of the exhaust gasses with the on board instruments, the HGA and solar panels, axial thrusters are canted 10° away from the Z-axis while the lateral thrusters are canted 5° away from the X-axis and 12.5° toward the Z-axis^[5]. This particular configuration of RCS is required since no RW nor any other type of active attitude control is present on the spacecraft: the ability of decoupling the forces and the momentum was thus needed. Lateral thrusters are denominated with letter "L" while axial thrusters are denominated with letter "A", as can be seen both from Figure 2.3 and Figure 2.4. This configuration increased the overall sturdiness of the propulsion system as "A" thrusters could be used as replacement of the ME for small manoeuvres. A simplified scheme of the propulsion system has been developed in Figure 2.5.

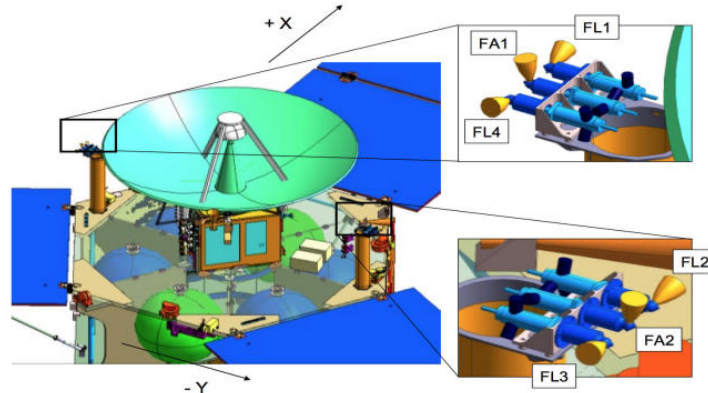


Figure 2.4: RCS Forward mount

2.2.2 Manoeuvre Implementation Modes

Juno's manoeuvres can be performed in two different modes: *vector-mode* and *turn-burn-turn*. The *vector-mode* consists of separated and coordinated axial and lateral burns from RCS thrusters. As seen in subsection 2.2.1, the thrusters are not exactly perpendicular one to the other, so during a *vector-mode* manoeuvre an induced axial ΔV is generated and must be compensated. The *turn-burn-turn* mode consists in a sequence of RCS and ME burns: first the spacecraft slews to the design spinning rate of 5 RPM, then the ME is ignited and the manoeuvre is performed. At last, the spacecraft slews back to its nominal spinning rate. This mode is used during all the ME burns. In this kind of manoeuvre the RCS uses the "L" thrusters on the REMs.

2.2.3 Tanks

Juno's tanks are equally distributed throughout its hexagonal shaped body. Four tanks are needed to store hydrazine and two tanks are needed to store the oxidizer. As can be seen from Figure 2.4, the oxidizer ones (green tanks) are located along the X-axis, while fuel ones (blue ones) are placed in the remaining bays. All six tanks work at 2.15 MPa, estimated as the sum of the nominal operational pressure of the ME and a small amount, 50 kPa, induced by the pressure losses of the system^[9]. On board tanks have a sphere-like shape: it allows to have the most internal volume with the lowest possible surface and so both weight and heat exchange are limited.

The two tanks^[13] containing the supercritical helium needed to pressurize the propellant system are assumed to be initially pressurized at 21.5 MPa, a value ten times higher than the nominal working pressure, and are placed near solar wing one and solar wing two. Unlike fuel and oxidizer tanks, helium ones do not have a sphere-like shape due to volume management inside the bays^[14]: cylindrical tanks allow to fill better the gaps present under the main tanks. The positioning of the pressurizer tanks breaks even more the symmetry of the mass distribution: this feature, in concomitance with the distribution of the propellant tanks, will make the COM shift not only along the Z-axis unless other precautions were made in placing other internal components.

A system of valves regulates the pressure inside the tanks to allow nominal operations of the ME and RCS. All the tanks are insulated from their surroundings and heating elements are present on both tanks and feeding lines to ensure safe and nominal temperature inlet for the whole propulsion system. One of the main problem with managing liquid in space is the need of guiding the propellants to the feeding lines of the engines to avoid mixture of gas and liquids during the injection in the combustion chamber, compromising the correct functioning of the propulsion system. Moreover, liquid propellants produce sloshing movements that could apply forces and moments inside the tanks, causing an unsteady oscillatory spin. Juno is a spin-stabilized spacecraft so the induced forces would cause a movement of nutation. A Propellant Expulsion Device (PED) is thus needed: the spinning of the spacecraft helps guiding the propellant to the most exterior part of the tanks were feeding lines are located^[15]. MEFs are tasks needed to flush the main propellant line in order to test the system after a long period of rest. In order to accomplish its mission, Juno holds about 2000 kg of propellant: about 1280 kg of fuel and 720 kg of oxidizer^[5]. A more detailed analysis of tanks will be conducted in subsection 2.3.1.

2.3 Reverse engineering of propulsion system

As described in subsection 2.2.3, the propulsion system counts four tanks for storing hydrazine, two tanks for storing NTO and two tanks for storing helium. To better understand the reasoning behind this choice, a reverse sizing for both the propellants and the pressurizer has been conducted given the data on the engines, the ΔV highlighted in Table 2.2 and the total dry mass M_{dry} ^[16] of the spacecraft. The whole process has taken into account the standardized margins from ESA.^[17] Since the actual mission has greatly deviated from its initial design, a second propellant sizing was also performed on the real manoeuvres up to 7th June 2021^{[5][6][18]} plus the required de-orbit to check the compliance with the design masses.

2.3.1 Fuel and oxidizer tanks sizing

1. To estimate the masses of the propellants, Tsiolkovsky rocket equation has been applied iteratively on the ΔV of the first column of Table 2.2. This process needs the dry mass $M_{dry} = M^{(0)}$ of the spacecraft as first input and starts from the last ΔV (the de-orbit burn) incrementing the computed total mass $M^{(i)}$ and the propellant mass $M_{p,me}^{(i)}$ or $M_{p,rcs}^{(i)}$ after each iteration.

$$M_{p,me}^{(i+1)} = M^{(i)} \cdot \left[\exp\left(\frac{1.05 \cdot \Delta V^{(i)}}{I_{s,me} \cdot g_0}\right) - 1 \right] + M_{p,me}^{(i)} \quad (2.2)$$

$$M_{p,rcs}^{(i+1)} = M^{(i)} \cdot \left[\exp\left(\frac{2 \cdot \Delta V^{(i)}}{I_{s,rcs} \cdot g_0}\right) - 1 \right] + M_{p,rcs}^{(i)} \quad (2.3)$$

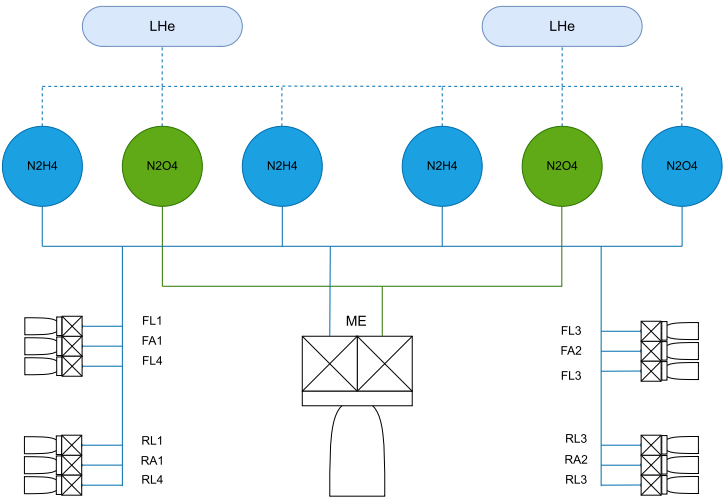


Figure 2.5: Propulsion system architecture
The diagram illustrates the Juno propulsion system architecture. It features a central Main Engine (ME) at the bottom. Above the ME are two rows of tanks. The top row consists of two green N2O4 tanks and two blue N2H4 tanks, connected to a central horizontal line. The bottom row consists of two blue N2H4 tanks and two green N2O4 tanks, also connected to the same central line. Two large blue ovals labeled 'LHe' are positioned above the top row of tanks. Feeding lines (FL) and return lines (RL) are shown connecting the tanks to the ME. Specific valve configurations are labeled FL1, FA1, FL4, RL1, RA1, RL4, FL3, FA2, FL3, RL3, RA2, RL3.

$$M^{(i+1)} = M^{(i)} + M_{p,me}^{(i)} \quad \text{or} \quad M^{(i+1)} = M^{(i)} + M_{p,rcs}^{(i)} \quad (2.4)$$

where the respective formula is applied based on which engine type performs the i-th manoeuvre.

2. From the final $M_{p,me}$ and $M_{p,rcs}$, the masses of fuel and oxidizer are then computed. This is done by knowing the nominal O/F ratio (0.85) of the ME^[9] and that the RCS only uses hydrazine as propellant. Exploiting the density of the propellants, the total volumes for fuel and oxidizer are retrieved.

$$M_f = \frac{1}{O/F + 1} \cdot M_{p,me} + M_{p,rcs} \quad (2.5)$$

$$M_{ox} = \frac{O/F}{O/F + 1} \cdot M_{p,me} \quad (2.6)$$

The estimated masses are rather similar to the real ones, as it can be seen in Table 2.3.

	Estimated masses [kg]	Real masses [kg] ^[16]	Relative error [%]
M_f	1309.5	1280	2.304
M_{ox}	751.9	752	0.013

Table 2.3: Comparison between estimated and real masses

3. Having the total volumes of propellants, they have been split among the number of spherical tanks. Since the radius r_{tank} obtained for the two types of tanks are very similar and having two different tanks is inconvenient, the larger one was selected.

Fuel tank radius [cm]	Oxidizer tank radius [cm]
43.99	40.91

Table 2.4: Comparison between obtained radii

4. The pressure of the tanks p_{tank} is kept constant (as described in subsection 2.2.3). From the pressure and the volume of one tank, the required thickness t_{tank} can be computed by choosing the material, characterized by its density ρ and its tensile yield strength σ .

$$t_{tank} = \frac{r_{tank} p_{tank}}{2\sigma} \quad (2.7)$$

5. The dry mass of one tank is then computed to select the material:

$$M_{tank} = \frac{4}{3}\pi\rho[(r_{tank} + t_{tank})^3 - r_{tank}^3] \quad (2.8)$$

Three different materials have been taken into consideration, and the lighter configuration has been selected.

	Ti6Al4V	Al7075	Stainless steel
σ [MPa]	950	510	1400
ρ [kg/m ³]	4500	2810	8100
t_{tank} [mm]	0.50	0.93	0.34
M_{tank} [kg]	5.45	6.35	6.66

Table 2.5: Properties of the materials tested for the sizing of the tanks

2.3.2 Pressurizer tanks sizing

1. As a first approximation, the pressure for the helium tanks is supposed to be ten times the pressure for the propellant tanks p_{tank} , and helium is considered to be a perfect gas (actually it is in a supercritical state). The temperature T_{tank} for the tanks is assumed to be 20 °C. Starting from these assumptions, the mass and the volume

of the total required helium are computed as follows:

$$M_{He} = 1.2 \cdot \frac{p_{tank} \cdot 6V_{tank} \cdot \gamma_{He}}{(1 - 1/10) R_{He} T_{tank}} \quad (2.9)$$

$$V_{He} = \frac{M_{He} R_{He} T_{tank}}{10 p_{tank}} \quad (2.10)$$

2. Since the two tanks are cylindrical, the geometry is undefined given only the volume of one tank. To add the missing constraint, a minimization of the total surface is assumed, which can minimize the internal stress due to pressure and the heat transfer through the walls ([subsection 2.2.3](#)).

$$r_{tank,He} = \left(\frac{1/2 V_{He}}{2\pi} \right)^{1/3} \quad (2.11)$$

$$h_{tank,He} = \frac{1/2 V_{He}}{r_{tank,He}^2 \pi} \quad (2.12)$$

3. As already done in [subsection 2.3.1](#), the thickness $t_{tank,He}$ is computed for the materials in [Table 2.5](#) as:

$$t_{tank,He} = \frac{r_{tank,He} \cdot 10 p_{tank}}{2\sigma} \quad (2.13)$$

4. The dry mass of one tank is then computed to select the material:

$$M_{tank,He} = \rho h_{tank,He} \pi \left[(r_{tank,He} + t_{tank,He})^2 - r_{tank,He}^2 \right] + 2\rho t_{tank,He} r_{tank,He}^2 \pi \quad (2.14)$$

As for the propellants tanks, titanium alloy appears to be the lightest solution ([Table 2.6](#)). This is the material most likely used for the tanks on the real satellite, and it is the most widely used in space due to its high strength to mass ratio and corrosion resistance.

	Ti6Al4V	Al7075	Stainless steel
$t_{tank,He}$ [mm]	3.58	6.68	2.43
$M_{tank,He}$ [kg]	30.62	35.73	37.51

[Table 2.6](#): Thickness and mass of helium tanks for different materials

2.3.3 Computation of actual propellants usage

The second sizing relies on the same procedure highlighted in [subsection 2.3.1](#) with the difference that it starts from the launch mass $M_{launch} = M^{(0)}$ ^[16] and considers the ΔV from the second column of [Table 2.2](#) in chronological order. [Equation 2.2](#) and [Equation 2.3](#) are thus modified as follows:

$$M_{p,me}^{(i+1)} = M^{(i)} \cdot \left[1 - \exp\left(\frac{-\Delta V^{(i)}}{I_{s,me} \cdot g_0}\right) \right] + M_{p,me}^{(i)} \quad (2.15)$$

$$M_{p,rcs}^{(i+1)} = M^{(i)} \cdot \left[1 - \exp\left(\frac{-\Delta V^{(i)}}{I_{s,rcs} \cdot g_0}\right) \right] + M_{p,rcs}^{(i)} \quad (2.16)$$

where the ESA margins^[17] were not applied since the actually performed manoeuvre values were utilized. The real and consumed masses are reported in [Table 2.7](#).

	Real masses [kg]	Consumed masses [kg]	Remaining masses [kg]
M_f	1280	986	294
M_{ox}	752	560	192

[Table 2.7](#): Real and consumed propellants masses

The *remaining masses* column denotes the propellants masses still present in the spacecraft as of 7th June 2021, which are obtained by subtracting the calculated masses from the real ones. Since the de-orbit is mandatory its ΔV has been considered as a final real manoeuvre even though it hasn't happened yet.

Bibliography

- [1] Try Lam Theres D. Kowalkowski. "Launch Period Development for the Juno Mission to Jupiter". In: (2008).
- [2] United Launch Alliance. *Atlas V Juno*. Site: https://www.ulalaunch.com/docs/default-source/rockets/atlasvusersguide2010a.pdf?sfvrsn=f84bb59e_2. 2011.
- [3] Rick Nybakken. "The Juno Mission to Jupiter: A pre-launch update". In: (2011).
- [4] Paul F. Thompson et al. "Juno navigation for Jupiter orbit insertion". In: (2017).
- [5] Thomas A. Pavlak et al. *Maneuver Design for the Juno Mission: Inner Cruise*. AIAA space forum. Site: <https://arc.aiaa.org/>. 2018.
- [6] Paul W. Stumpf et al. *Maneuver Operations During Juno's Approach, ORBIT INSERTION, AND EARLY ORBIT PHASE*. JPL open repository. Site: <https://dataverse.jpl.nasa.gov/file.xhtml?fileId=58768&version=1.1&toolType=PREVIEW>. 2017.
- [7] S. Stephens. *Juno Mission Plan Document*. Planetary Data System. Site: https://pds.nasa.gov/ds-view/pds/viewMissionProfile.jsp?MISSION_NAME=JUNO. 2011.
- [8] Various. *Juno Mission and Trajectory Design*. Website. Site: <https://spaceflight101.com/juno/juno-mission-trajectory-design/>. 2024.
- [9] Nammo. *Leros 1b engine*. Journal of Geophysical Research: Planet. Site: <https://www.nammo.com/wp-content/uploads/2021/03/2021-Nammo-Westcott-Liquid-Engine-LEROS1B.pdf>.
- [10] Dr. Edward. J. Wucherer al. *Improving and Testing S-405 Catalyst*. AIAA space forum. Site: <https://arc.aiaa.org/doi/epdf/10.2514/6.2013-4053>. 2013.
- [11] Aerojet Rocketdyne Propulsion plays role in Juno mission. Online Communication. Site: <https://www.proquest.com>. 2016.
- [12] *MR-111C datasheet*. Site: <http://www.astronautix.com/m/mr-111.html>.
- [13] *Launch*. Site: <https://www.missionjuno.swri.edu/launch>.
- [14] Dr. Mary M. Mellott et al. *NSSDCA/COSPAR ID: 2011-040A*. Nasa SSDCA. Site: <https://nssdc.gsfc.nasa.gov/nmc/spacecraft/display.action?id=2011-040A>. 2022.
- [15] Sathya Gangadharan et al. *Modeling of Fuel Slosh in a Spin Stabilized Spacecraft with On-Axis Propellant Tanks Implemented with Diaphragms*. AIAA Modeling and Simulation Technologies Conference 10 - 13 August 2009, Chicago, Illinois. Site: <https://arc.aiaa.org/>. 2009.
- [16] NASA JPL. *Juno Quick Facts*. Site: https://www.jpl.nasa.gov/news/press_kits/juno/facts/. 2011.
- [17] European Space Agency. "Margin philosophy for science assessment studies". In: (2012).
- [18] Thomas A. Pavlak et al. "Juno trajectory redesign following PRM cancellation". In: (2017).

Homework 3

Notation

TMTC	Telemetry and Telecommand	BVR	Block-V Receivers
HGA	High Gain Antenna	FTS	Frequency and Timing Subsystem
MGA	Medium Gain Antenna	BER	Bit Error Rate
LGA	Low Gain Antenna	MWR	Micro Wave Radiometer
TLGA	Toroidal Low Gain Antenna	DSS	Deep Space Station
TWTA	Traveling Wave Tube Amplifier	RSR	Radio Science Receiver
ALGA	Aft Low Gain Antenna	D/L	Downlink
FLGA	Forward Low Gain Antenna	U/L	Uplink
DSN	Deep Space Network	P_{rx}	Power received [W]
DSM	Deep Space Manuevers	P_{tx}	Power transmitter [W]
JOI	Jupiter Orbit Insertion	G_{rx}	Gain receiver [-]
PRM	Period Reduction Manuever	G_{tx}	Gain transmitter [-]
SDST	Small Deep Space Transponder	L_c	Cable losses [-]
SSPA	Solid State Power Amplifier	L_s	Space losses [-]
DPM	Digital Processing Module	$L_{p,tx}$	Receiver pointing losses [-]
F1	Fundamental frequency	$L_{p,rx}$	Transmitter pointing losses [-]
DOR	Differential One-way Ranging	L_a	Atmospheric losses [-]
RHCP	Right-Hand Circular Polarization	L_{cv}	Antenna cover losses [-]
LHCP	Left-Hand Circular Polarization	k	Boltzmann constant [J/K]
RF	Radio Frequency	T_{eq}	Equivalent temperature [K]
OTM	Orbit Trim Manuever	R	Datarate [bps]
BPSK	Binary Phase Shifting Keying	N_0	Noise spectral density [W/Hz]
MFSK	Multiple Frequency Shift Keying	E_b	Energy per bit [J/bit]
AWVR	Advanced Water Vapor Radiometer	r_{JE}	Juno-Earth distance [AU]
LNA	Low Noise Amplifier	f	Frequency [Hz]
KaTS	Ka-band Translator	d_g	Ground antenna diameter [m]
IF	Intermediate Frequency	η	Pointing error [-]
RF	Radio Frequency	G	Antenna gain [dB]
RS	Radio Science	θ_{bw}	Antenna beamwidth [deg]
SR	Science Receiver	EIRP	Equivalent isotropic radiated power [dBm]
OLR	Open Loop Receivers	$(.)_{mar}$	Margin value
VLBI	Very Long Baseline Interferometry		

3.1 TMTc system architecture

The Juno TMTc subsystem purpose is to communicate data about the status of the spacecraft, to send scientific data and to receive commands, from and to the DSN antennas. Both the uplink and downlink are performed in X-band frequency: 8.4 GHz for downlink and 7.1 GHz for uplink. The selection of this band was imposed by pre-existing DSN facilities. It allows to transmit relatively large datarates over wide distances with low atmospheric attenuation. One of the main goals of the mission is to study Jupiter's gravity field: this is accomplished by exploiting the difference in Doppler effect of the telecommunication from the model and the real jovian gravity field. Due to the harsh environment that Juno faces and the need to measure precisely the residual frequency, transmission on both X-band and Ka-band during gravity science is needed. The Ka-band has an advantage on the X-band since the noise due to interplanetary plasma is inversely proportional to the wavelength, higher on the Ka-band, making the measurements more accurate^[1]. For this reason, the HGA can operate in 3 different modes:

- X/X: uplink and downlink are coherent and performed in X-band;
- X/X & X/Ka: simultaneous transmission on X-band (uplink and downlink), together with a coherent Ka-band downlink at 32 GHz and X-band uplink;
- X/X & Ka/Ka: phase coherent X-band uplink and downlink together with a phase coherent Ka-band uplink at 34 GHz and downlink.

In order to calibrate the dispersive noise contribution when receiving X-band and Ka-band signals simultaneously, Juno is equipped with a KaTS. This instrument is capable of receiving a Ka-band uplink unmodulated carrier from DSN and to generate a Ka-band downlink unmodulated carrier coherent with the uplink to maintain the phase stability from ground communication, on which the quality of the experiments depends^[2].

Five antennas are mounted on-board Juno with different orientations, positions and capabilities: one HGA, one MGA, two LGAs and one TLGA.

In order to process different signals at different frequencies, Juno has two SDSTs, capable of performing different tasks. The prime unit provides X/X and X/Ka link, whereas the secondary unit only operates on the single X-band. Each SDST is composed of four different units: the DPM, the down converter, the power converter and the exciter unit. The DPM is responsible for managing the data incoming from the down-converter, encoding them and providing X-band baseband telemetry. The down-converter module converts the incoming 7.1 GHz signal into an intermediate frequency at 4/3 F1, where F1, approximately 9.55 MHz, is the fundamental frequency from which up and downlink frequencies are derived. The power converter is responsible for supplying a steady voltage to all SDST modules and the exciter is responsible for taking as an input telemetry, DOR, ranging and for phase-modulating the downlink carrier^{[1][2]}.

The SDST is responsible for generating the X-band downlink carrier by coherently multiplying the frequency of the uplink carrier by a turn-around ratio of 880/749. All X-band signals are amplified by one of two-redundant 25 W TWTAs^[2]. This kind of technology was imposed by the high power demand for the link on this frequency. For the Ka-band transmission, SSPA was preferred due to less required power for transmission and weight saving.

Before the transmission of the signal actuated by the antennas, the data is manipulated with modulation and encoding techniques. The chosen modulation is BPSK which ensures a good use of spectrum and relatively low BER. Moreover, it was flight-proven and requires less complex on-board architecture. Encoding is performed in two ways depending on the type of the transmission: the Reed-Solomon algorithm allowed lower BER to be reached, while Turbo code 1/6 was used for larger datarates of transmission.

3.1.1 HGA

The HGA^{[2][3]} is the principal means of communication with Earth throughout most of the cruise and science mission. It is mounted on the forward deck, aligned with the spin axis of the spacecraft, as shown in Figure 3.1. Due to the significant distance between Juno and DSN antennas and the limited transmitter power, HGA gain maximization was a priority. Constraints on dish dimension and in the attitude control of the spin-stabilized spacecraft were present: the Atlas V fairing limited the HGA dish diameter to 2.5 meters, then the presence of massive solar arrays prevented pointing the main beam to anything tighter than about $\pm 0.25^\circ$. The latter limitation would have led to an insufficient gain in the HGA, preventing closing the link with Earth. The most limiting factor in designing

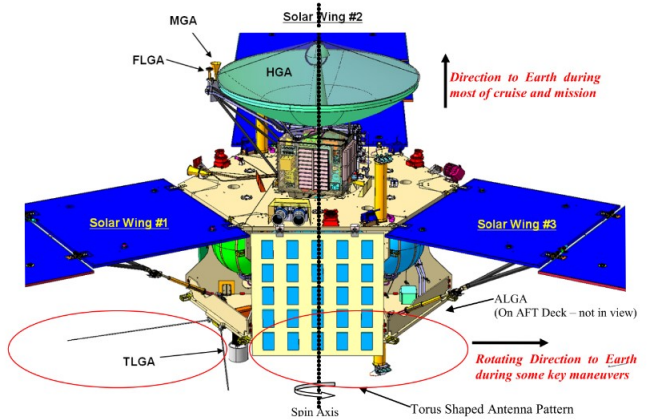


Figure 3.1: Location of telecommunication antennas

the HGA was the need of both transmitting and receiving on X-band and Ka-band without affecting excessively the performance of any signal. Because of these requirements, a dual-reflector Gregorian-style optics was installed. The latter consists in a parabolic main reflector and an elliptical sub-reflector, making the whole system low in mass and compact^[3]. The outer annular region is made so that the radiated field of the X-band is 180° out of phase with the inner region aperture field: the resulted beamwidth of the Ka-band is approximately the same as the X-band one. This modification created almost no performance degradation on X-band link. Based on frequency and operational mode, different polarizations are utilized: X-band uses RHCP for both uplink and downlink, while Ka-band uses RHCP for downlink and LHCP for uplink^[2]. Required gain is about 44 dB for the X-band in both uplink and downlink and around 47 dB for the Ka-band.

Other limiting factors were present in designing the HGA in terms of thermal and structural constraints: the stability in pointing at low temperatures is granted by a very stiff graphite composite. Moreover, the HGA's shielding from the high temperature oscillation (from -175°C to 135°C) and radiation dose experienced during both cruise and jovian phase is accomplished using a thermal blanket made of a carbon-loaded Germanium-Kapton material^{[3][4]}. As a result, the performances were only affected by a loss of 0.25 dB at X-band and a 0.5 dB loss on the Ka-band.

3.1.2 MGA & LGAs

One MGA and two LGAs are mounted on-board Juno. Their position can be seen in [Figure 3.1](#). Both types of antennas come as legacy from previous missions. LGAs were previously used on the Mars Reconnaissance Orbiter and as part of a family of antennas used for deep space missions. Instead, MGA was used in Mars Exploration Rover cruise stage^[3].

The MGA is a conical horn-style antenna and it is aligned with the +Z-axis as the HGA and it is used during cruise, safe mode and manoeuvres. It is capable of both LHCP and RHCP for redundancy and communicates with the DSN only in X-band, using the same frequencies of the HGA. This antenna provides at least 18.1 dBic while receiving and 18.8 dBic while transmitting, with a 3 dB beamwidth of $\pm 10.3^\circ$ and $\pm 9.3^\circ$ respectively.

The two identical and coupled LGAs are pointing in opposite directions, one mounted on the forward deck (FLGA) and the other on the aft deck (ALGA). LGAs have a choked horn design and transmit on the same X-band frequencies as the MGA and HGA. While delivering inferior performances regarding the minimum required boresight (8.7 dB in receiving and 7.7 dB in transmitting), they operate with a higher 3 dB beamwidth at around $\pm 40^\circ$ ^[2].

The LGAs are used mainly at a distance inferior to 0.5 AU from Earth and during manoeuvres, when orientation of the spacecraft does not allow HGA communications due to sun-pointing requirement. Throughout main engine burns, the MGA is used in sequence with HGA and TLGA. This suit of antennas is also used during MWR science configuration.

3.1.3 TLGA

The TLGA is placed on the aft deck of Juno, aligned with solar wing #1. This antenna works at the same X-band frequency of the other antennas but differs from them since it has a bi-conical horn design and it is able to produce a RHCP radial pattern around Juno's spin axis: this characteristic is needed to ensure continuous coverage during all critical events, such as the DSMs, JOI, PRM and OTMs, when the attitude does not allow for direct Earth pointing. This antenna transmits only in a carrier or subcarrier configuration, where no ranging nor telemetry signals are modulated onto the carrier. During ME manoeuvres Juno encodes MFSK tones by modulating a varying frequency subcarrier onto the carrier. Every subcarrier frequency is associated to a particular event or state of the spacecraft and allows a complete knowledge of Juno's health. The particular advantage of using a subcarrier is the capability of providing an additional channel of transmission: it allows different signals to be received together as one and then to be separated out by the receiver.

A toroidal antenna pattern can be produced by a dipole, but this design limits heavily the maximum gain reachable to around 2.2 dB, which is insufficient to provide communications between Juno and Earth. Thus, a bi-conical parabolic-shaped antenna with corrugated horn has been developed, allowing for a compact and efficient design: this configuration achieves values lower than 20 dB in return losses over the entire used X-band^[3]. The RHCP pattern is achieved through a four-layer meander-line polarizer, built to minimize RF losses. As the HGA described in [subsection 3.1.1](#), the TLGA is also covered in a Germanium-Kapton blanket to minimize high energy electrons' flux. Gains required for the TLGA are of 5.5 dBic while receiving and 6.5 dBic while transmitting, with a beamwidth of $\pm 10^\circ$ in both reception and transmission at $\pm 90^\circ$ with respect to the boresight angle^[2].

3.1.4 Ground stations

In order to retrieve data, Juno relies on the antennas of NASA's DSN, a system of three complexes spread around the globe, separated by approximately 120° in longitude: one is located in Goldstone, California; one in Madrid, Spain; the last one in Canberra, Australia. This configuration allows for constant observation of spacecraft while Earth rotates, as can be visualized in [Figure 3.2](#). Each site is fitted with one 70-meter diameter antenna and a set of 34-meter diameter antennas. At Ka-band, the beamwidth of the latter antennas is 4 times narrower than the X-band beamwidth (0.016° vs. 0.077° respectively), making the pointing critical to establish a stable link with the spacecraft.

All antennas are capable of receiving and transmitting in X-band, however only the smaller ones are also capable of receiving in Ka-band. DSS-25 antenna in Goldstone is the sole capable of Ka-band uplink: all Juno's closest approach periods to Jupiter are planned such that this particular antenna is in sight.

Since the troposphere introduces delays in the Doppler signal path, in order to retrieve a more accurate reading during gravity science, DSS-25 is equipped with a AWVR that measures the wet component of the troposphere and various frequencies, including 31.4 GHz, where Ka-band signal are performed. The wet component delays are statistically combined with data considering effects from surface meteorology to have a full evaluation of the delays in the Doppler signals^[5].

During communications, the signal is received by the antennas and then amplified by the LNA into an IF (at 300 MHz) easier to be carried by cables rather than a RF, that needs waveguides. Depending on the flexibility needed, an open-loop or closed-loop or monopulse closed-loop can be used for signal processing. There have been three types of open-loop receivers during Juno era, all functioning in similar capacities: RSR, VLBI, WVSR. The last two have been recently replaced by a more recent OLR due to obsolescence issues in maintenance^[6]. Open-loop receivers opt for a specific band of frequencies to amplify and then transmit the data to RS or VLBI equipment for processing and storage. They are used during high-dynamic or low-signal level events because of their ability to best guess the frequency of the received signal in order to sample the entire spectrum around the spacecraft's center frequency. Regarding closed-loop receivers, they are based on the advanced technology of BVRs, in which the spacecraft's downlink is selected and received. BVRs are able to detect subcarriers carrying telemetry or ranging data and to decode and process them. A program known as *conscan*^[7] is in charge of observing the strength of the receiver's signal to optimize the antenna's pointing via small circular movements. The usage of *conscan* during VLBI or RS operations is discouraged due to variations in signal levels, in its place a monopulse closed-loop receiver is used to optimize Ka-band reception. The monopulse system compares the gain and the phase of the received Ka-band signal to estimate needed corrections in the antenna's pointing to improve signal-to-noise ratio by 1÷3 dB-Hz^[1].

X-band and Ka-band signals are generated by the FTS, which relies on a hydrogen maser clock to maintain a stable reference frequency. The X-band exciter and Ka-band exciter generate an uplink carrier signal which is amplified by the transmitters. The Juno spacecraft then receives these signals and phase-coherently retransmits them to the DSN antenna. In Figure 3.3 it is possible to observe a simplified scheme of Juno's communication architecture.

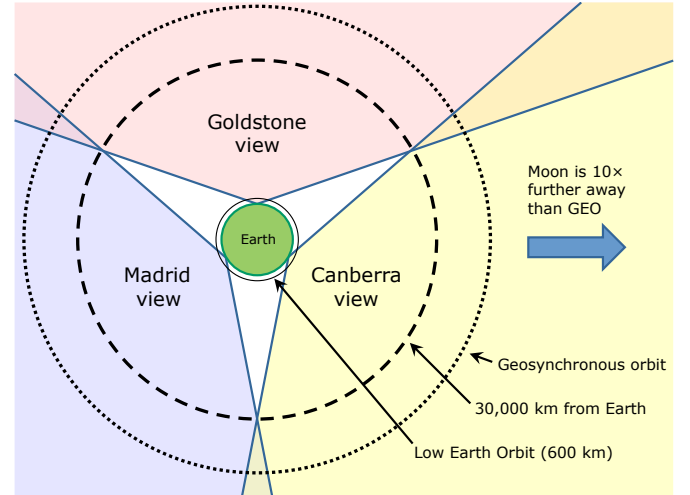


Figure 3.2: DSN coverage



Figure 3.3: Ground Station and Juno communication scheme

3.2 Phases breakdown

The satellite utilizes all the antennas throughout the different phases of the mission. During each one, the TMTC system must satisfy different linking requirements. The main phases are depicted in time in Figure 3.4 and then briefly discussed in Table 3.1.



Figure 3.4: Antennas operability during mission

Phase	Downlink/Uplink [bps]	Phase summary
Initial Acquisition	1745 / -	Initial acquisition performed through LGAs (zoom on Figure 3.4). Reed-Solomon coding was used.
Cruise	100 / 7.8125	Ranging is on during the whole cruise. Since Juno has to point the Sun, HGA is not usable during fly-by so all the other antennas are sequentially employed (Figure 3.4).
Orbital Operations	$1.8 \cdot 10^4$ / 2000	This is the most demanding phase, it requires at least 18 kbps in downlink through HGA. Also MGA and TLGA are used during OTMs, the latter only for tones (Figure 3.4).
Critical Event Coverage	- / -	No data during these phases, just tones through TLGA.
Safe Mode	10÷40 / 7.8125	Downlink datarate may be changed by flight software. Ranging is switched off during this mode.

Table 3.1: Summary of data links during mission phases^[2]

3.3 Reverse sizing of the HGA

The reverse sizing of the HGA is based on the link budget equation that represents a power balance between the transmitted signal and the receiver noise. The same equation can be applied on both uplink and downlink. It is valid for all the architectures, both that transmit data or tones.

$$\frac{P_{rx}}{N_0} = \frac{P_{tx}G_{tx}G_{rx}L_{tot}}{kT_{eq}} > \left(\frac{P_{rx}}{N_0} \right)_{min} \quad (3.1)$$

For antennas that broadcast data, an additional equation is used to constrain the sizing.

$$\frac{E_b}{N_0} = \frac{P_{tx} G_{tx} G_{rx} L_{tot}}{k T_{eq} R} > \left(\frac{E_b}{N_0} \right)_{min} \quad (3.2)$$

L_{tot} considers the following losses:

$$L_{tot} = L_c \cdot L_s \cdot L_{p,tx} \cdot L_{p,rx} \cdot L_a \cdot L_{cv} \quad (3.3)$$

For each communication link, different minimum required ratios are defined. In particular, $\frac{E_b}{N_0}$ must also satisfy the Shannon theorem by ensuring a value higher than -1.59 dB. The HGA, as described in subsection 3.1.1, is used for the downlink of telemetry and scientific data during the science orbits around Jupiter. It has been sized in the following scenario:

- the maximum distance from Earth $r_{JE} = 6.5$ AU;
- the minimum datarate $R = 18$ kbps has to be ensured regarding the distance.

From the literature, some other parameters were recovered and reported in Table 3.2. The results of the sizing are shown in Table 3.3. In particular, some margin is present on both X-band and Ka-band. Since the X-band is the only one transmitting data, Figure 3.5 and Figure 3.6 focus on the margin of the downlink. The principal loss of the link is given by the distance, so the two design parameters have been described as a function of it.

	X-D/L	X-U/L	Ka-D/L	Ka-U/L
f [GHz]	8.4	7.1	34.4	32.1
R [kbps]	18	2	–	–
d_{HGA} [m]	2.5			
d_g [m]	34			
P_{tx} [W]	25	$1.8 \cdot 10^4$	2.5	$1.8 \cdot 10^4$
η_{HGA} [deg]	0.25			
η_g [deg]	$4 \cdot 10^{-3}$		$2 \cdot 10^{-3}$	
L_c [dB]	-2	–	-2	–
L_a [dB]	-0.2		-1.09	
L_{cv} [dB]	-0.25		-0.5	
T_{eq} [K]	21	401.25	21	770.63
$(\frac{P}{N_0})_{min}$ [dB-Hz]	43.64	49.13	26.50	42.57
$(\frac{E_b}{N_0})_{min}$ [dB]	-0.1	9.6	–	–

Table 3.2: HGA data for sizing^[2]

	X-D/L	X-U/L	Ka-D/L	Ka-U/L
G_{HGA} [dBi]	44.25	42.79	56.50	55.90
G_g [dBi]	66.93	65.47	79.17	78.57
$\theta_{bw,HGA}$ [deg]	0.932	1.10	0.438^I	
$\theta_{bw,g}$ [deg]	0.069	0.081	0.017	0.018
L_s [dB]	-290.63	-289.17	-302.88	-302.28
L_p [dB]	-0.904	-0.646	-4.09	-4.51
$EIRP$ [dBm]	85.98	138.02	87.98	151.12
N_0 [dBm/Hz]	-185.38	-172.57	-185.38	-169.73
P_{rx} [dBm]	-138.83	-109.46	-140.90	-101.36
$\frac{P}{N_0}$ [dB-Hz]	46.55	63.11	44.47	68.38
$(\frac{P}{N_0})_{mar}$ [dB-Hz]	2.91	13.98	17.97	25.81
$\frac{E_b}{N_0}$ [dB]	4.00	30.10	–	–
$(\frac{E_b}{N_0})_{mar}$ [dB]	4.10	20.50	–	–

Table 3.3: Results for HGA

^I This value was recovered from a graphical analysis of the HGA Ka-band gain pattern.^[2]



Figure 3.5: Datarate as function of distance by fixing $E_b/N_0 = -0.1$ dB

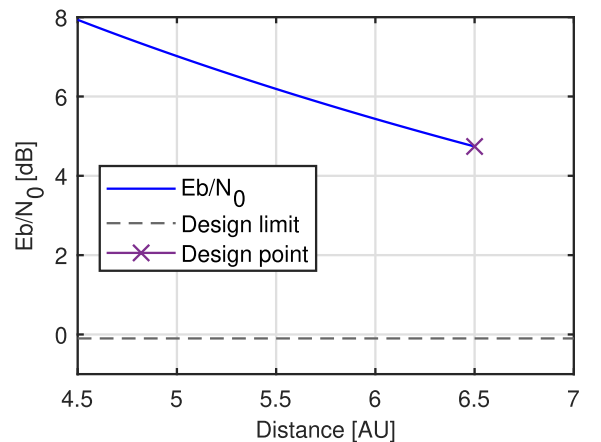


Figure 3.6: Energy per bit to noise ratio as function of distance by fixing $R = 18$ kbps

Bibliography

- [1] Dustin Buccino et al. "Juno Gravity Science: Five Years of Radio Science Operations with Ka-band Uplink". In: (2022).
- [2] Anthony P. Mittskus et al. "Juno Telecommunications". In: (2012).
- [3] Anthony P. Mittskus et al. "Telecommunications Antennas for the Juno Mission to Jupiter". In: (2012).
- [4] *DuPont™ Kapton*. Site: kapton.com.
- [5] Dustin Buccino et al. "Calibration and Performance of Juno Radio Science Data". In: (2020).
- [6] Dustin Buccino et al. "Detecting Juno's "Heartbeat": Communications Support during Critical Events of the Juno Mission". In: (2020).
- [7] *Deep Space Network*. Site: <https://science.nasa.gov/learn/basics-of-space-flight/chapter18-3/>.

Homework 4

Notation

AOCS	Attitude and Orbit Control System	SSS	Spinning Sun Sensor
TCS	Thermal Control System	IMU	Inertial Measurement Unit
TMTC	TeleMetry and TeleCommand	ASC	Advanced Stellar Compass
PS	Propulsion System	CHU	Camera Head Unit
P/L	PayLoad	MAG	MAGnetometer
S/C	SpaceCraft	FGM	FluxGate Magnetometer
SPM	Sun Pointing Mode	SSIRU	Scalable Space Inertial Reference Unit
EPM	Earth Pointing Mode	HAMRR	High Accuracy Mode Rate Range
GRAVM	GRAVity science Mode	MIB	Minimum Impulse Bit
MWRM	MicroWave Radiometer Mode	AD	Attitude Determination
TBTM	Turn-Burn-Turn Mode	ME	Main Engine
VECM	VECtor Mode	FOV	Field Of View
SCM	Spin Change Mode	RCS	Reaction Control System
SM	Safe Mode	CMG	Control Moment Gyro
SPE	Sun Probe Earth	REM	Rocket Engine Module
APE	Absolute Performance Error	TRL	Technology Readiness Level
EGA	Earth Gravity Assist	SRP	Solar Radiation Pressure
PJ	PeriJove	GG	Gravity Gradient
DSM	Deep Space Manoeuvre	HGR	Hemispherical Resonator Gyroscope
JOI	Jupiter Orbit Insertion	HGA	High Gain Antenna
PRM	Period Reduction Manoeuvre	MGA	Medium Gain Antenna
OTM	Orbit Trim Manoeuvre	LGA	Low Gain Antenna
TCM	Trajectory Correction Manoeuvre	TLGA	Toroidal Low Gain Antenna
IC	Inner Cruise	OT	Operational Temperature
OC	Outer Cruise	PC	Power Consumption
D/L	DownLink	ARW	Angle Random Walk
MWR	MicroWave Radiometer	ΔV	Velocity change [m/s]
SRU	Stellar Reference Unit	F_s	Solar constant [W/m ²]
TDI	Time Delay Integration		

4.1 Introduction of AOCS

The Attitude and Orbital Control System of Juno comprehends various sensors and actuators that are vital to maintain the satellite in operability conditions and to execute all the basic tasks. In this chapter, the main modes of the satellite are deduced through the analysis of the mission already done in previous chapters. These modes will be then arranged on the timeline consequently. Based on the identified modes and pointing budget, the architecture of the actual system will be presented and then progressively analyzed, verifying the compliance with the previously found requirements. Finally, a reverse sizing of AOCS will be carried out.

4.2 Breakdown of Juno modes

Throughout the mission phases, Juno has to accomplish different tasks through various modes. The principal ones that have been identified are here described.

4.2.1 Sun Pointing Mode (SPM)

This mode aims at pointing the spin axis of S/C (+Z axis) to the Sun. This mode is used in order to:

- keep the solar panels pointed to the Sun to provide energy; this is even more crucial in the initial phases of the mission, when all the system checkouts have to be performed;
- thermally protect the satellite's vault using the HGA as a shield when the satellite is relatively close to the Sun.

This mode is applied mainly when the SPE angle is too large to ensure the communication through the HGA. This condition occurs during the first phases of the mission and nearby the EGA, when the satellite is in proximity of Earth and relatively close to the Sun. The LGAs (mainly the TLGA) are therefore used during this mode to communicate with ground.

The pointing requirement (APE) for this mode is not very strict since the solar panels are sized for much higher distances and can provide enough energy, the LGAs have a wide beamwidth to communicate with ground and the HGA is large enough to protect the vault. The spin rate of the satellite is set to 1 RPM for this interplanetary mode. This improves the passive stability of the pointing, reducing the burden on the active attitude control. To assess a preliminary APE for this mode, the thermal requirement has been interpreted as visible in Figure 4.1.

This condition has been selected among the others since power generation results not to be critical at the maximum distance at which this mode is triggered ($\lesssim 1.4$ AU)^[1]. The shadow of the antenna shall cover entirely the vault below it as a first and conservative approximation. The resulting APE angle is reported in Table 4.1. This value is relatively high with respect to other more restrictive modes, hence it won't be the sizing factor for the choice of AOCS hardware.



Figure 4.1: Sketch for APE evaluation

4.2.2 Earth Pointing Mode (EPM)

The EPM is an interplanetary mode analogous to the SPM, where the +Z axis of the S/C is pointed to Earth. It triggers when the distance from the Sun is high enough to ensure a safe thermal dissipation without the aid of the HGA (≈ 1.4 AU)^[1]. Moreover, the S/C will be far enough from Earth to ensure both HGA communications and the fulfillment of power requirements, hence the SPE is low. The APE for this mode depends on the antenna that will be pointed to Earth: when the switch from SPM happens, the MGA is first pointed to Earth and subsequently the HGA is activated. The most restrictive APE is given by the beamwidth of HGA. This mode is always relative to the interplanetary phase and is the main one used throughout the cruise. The spin rate of 1 RPM ensures stability of the axis that is pointing to Earth.

4.2.3 GRAVity science Mode (GRAVM)

The GRAVM is the principal mode for science operations orbits around Jupiter. It aligns the +Z axis towards Earth in order to communicate and to perform the gravity experiment with the HGA. Hence, the APE is related to the antenna beamwidth specification, moreover the SPE angle is always low enough ($\lesssim 10^\circ$)^[2] to ensure enough power generation from the solar cells. The spin rate for this mode is fixed at 2 RPM to ensure payload requirements and higher stability to the axis pointing, which is more perturbed due to the vicinity to Jupiter.

4.2.4 MicroWave Radiometer Mode (MWRM)

The MWRM is the secondary mode for science operations orbits around Jupiter. It aligns the +Z axis orthogonally to the orbital plane in order to nadir point the dedicated instrumentations, which are placed on the lateral surfaces of the S/C. The spinning axis is off-set from the Earth direction of $24^\circ \div 27^\circ$ ^[3]. The MWR orbits are carried out at the early stages of the Juno mission due to the accentuated degradation of the MWR payload. Furthermore, the mode occurs only around the PJ passage to acquire data without D/L. To send the information, Juno switches to GRAVM at the end of the experiment in order to align HGA and MGA towards Earth^[2]. The spin-rate is nominally set at 2 RPM for the same reasons highlighted in the GRAVM. The need to have a dedicated mode for the MWR experiment rises from the requirements on the payload itself. In particular, the MWR antennas shall follow the S/C ground track on Jupiter within an aperture of $\pm 5.4^\circ$, which is imposed by the beamwidth of the smallest one^[4]. The latter angle can be identified as the APE for this mode.

4.2.5 Turn-Burn-Turn Mode (TBTM)

The TBTM is performed to align the main engine (-Z axis) with the ΔV direction of the ME manoeuvre (DSMs, JOI, PRM). In particular, a slew manoeuvre of approximately 90° with a rate of $0.1^\circ/\text{s}$ is first performed. The SRUs are deactivated in order to avoid damaging the optics since they could point at the Sun. The thrusters are also activated to spin-up the angular rate at 5 RPM to ensure stability throughout the ME burn. During this time, the only communication link with Juno is through tones via TLGA. The end of operation of the ME is followed by the decrease of the spin rate to 1 or 2 RPM, depending on the mission phase. The APE for this mode is related to the precision required by the alignment of the ME. Since from literature no specific requirement was mentioned, a numerical evaluation was conducted in order to enlighten the effects of a misalignment from the nominal ΔV . In particular, the manoeuvres affected by this uncertainty are:

- **DSM-1:** an error on this manoeuvre could be easily solved during DSM-2, so it is not critical in APE evaluation;
- **DSM-2:** an error on this manoeuvre could lead to a failure on targeting Earth for EGA, since the following TCMs could not be sufficient to correct the trajectory;
- **JOI:** a contained error in the direction for this manoeuvre unlikely could lead to a catastrophic failure of the mission; instead the error could be corrected later by OTMs;
- **PRM:** as for the JOI, the error could be fixed easily during the next phases of the mission.

From these observations, the DSM-2 was selected as the most critical manoeuvre, hence it was better analyzed through numerical simulation. From ephemeris, the velocity vector after DSM-2 was taken as the nominal one. Then, in order to add the error due to APE, the nominal velocity was shifted within a cone of semi-aperture α_{APE} without changing the magnitude and then propagated until the date of the nominal EGA. Two values of α_{APE} were tested through this method, results can be seen in Figure 4.2 and Figure 4.3.

TCMs are performed throughout the interplanetary phase to correct the path, nevertheless their magnitude is limited to $\approx 9 \text{ m/s}$ ^[5]. For this reason a $\alpha_{APE} = 0.25^\circ$ was chosen to ensure a certain precision on TBTM.



Figure 4.2: Simulation results for $\alpha_{APE} = 0.25^\circ$



Figure 4.3: Simulation results for $\alpha_{APE} = 5^\circ$

4.2.6 VECtor Mode (VECM)

The VECM is performed for OTM and TCM with RCS only. The +Z axis pointing is maintained (Earth or Sun depending on the phase) and the same for the spin rate (1 or 2 RPM for interplanetary or science phase respectively). The direction of the burn is then decomposed into two directions (axial and lateral). The APE during this mode is inherited from the current phase.

4.2.7 Spin Change Mode (SCM)

Due to the nature of the spin-stabilized S/C, a control mode on the angular velocity is mandatory. The SCM is performed through RCS and it can be requested by other modes (TBTM) or executed by itself during cruise (before and after the fly-by). The Juno nominal spin rates are:

- 1 RPM for the interplanetary cruise;
- 2 RPM for the science orbits and the EGA (for payload requirements and pointing stability respectively);
- 5 RPM for the ME manoeuvres (for stability of the ΔV direction).

The tolerance on the spin rate is ± 0.05 RPM^[3].

4.2.8 Safe Modes (SM)

Safe modes are mainly divided into two different types, depending on whether three-axis attitude knowledge is retained or not.

- **SM-1:** the attitude is known, so the satellite maintains its current pointing (Earth or Sun). The required APE is inherited from the particular pointing in which the mode was triggered.
- **SM-2:** the attitude knowledge is lost. In this critical eventuality, the +Z axis will cone within 2° around the Sun direction. The APE is not specified for this configuration since it cannot be assured. The LGAs could be used to communicate thanks to their large beamwidth.^[6]

4.2.9 Pointing budget & Phases/AOCS modes correlation

	SPM	EPM	GRAVM	MWRM	TBTM	VECM	SCM	SM-1
TCS	$APE \leq 25^\circ$	-	-	-	-	$APE \leq 25^\circ$	-	$APE \leq 25^\circ$
TMTC	-	$APE \leq 0.25^\circ$	$APE \leq 0.25^\circ$	-	-	$APE \leq 0.25^\circ$	-	$APE \leq 0.25^\circ$
PS	-	-	-	-	$APE \leq 0.25^\circ$ rate = $0.1^\circ/\text{s}$	-	-	-
P/L	-	-	$APE \leq 0.25^\circ$	$APE \leq 5.4^\circ$	-	-	$APE \leq 0.05$ RPM	-

Table 4.1: Pointing budget for AOCS

Table 4.1 synthesizes the pointing requirements of the main subsystems of the S/C in terms of performance for the AOCS. The empty cells in the table indicate no influence of the subsystem in the pointing budget for the selected mode. It can be noticed that the most stringent pointing APE is 0.25° (inherited by the beamwidth of HGA), which is compliant with the precision obtainable by the spin-stabilized thruster configuration of Juno coupled with the chosen sensors. For TBTM the same APE as the HGA was arbitrarily selected after the analysis described in subsection 4.2.5. In particular, this choice has consequences on the required precision for the sensors: since during TBTM the SRU must be deactivated, the other sensors have to be selected in order to keep the same precision. In Figure 4.4 the sequence of the different modes for the nominal mission is correlated with the phases. The OTMs performed in VECM during science phase are not shown for sake of clarity.

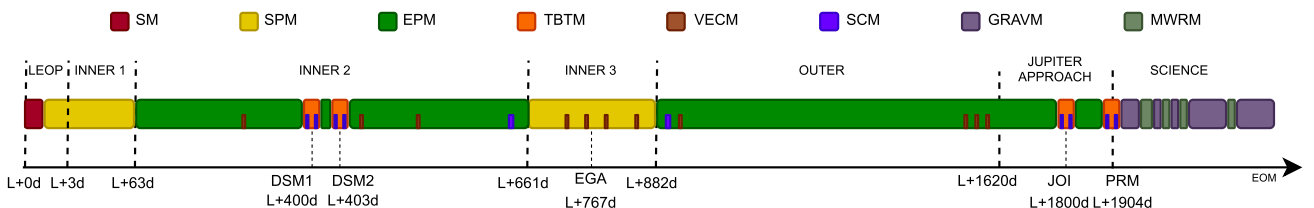


Figure 4.4: Timeline for mission phases (not in scale)

4.3 Architecture and rationale of AOCS

To achieve the required performance and capabilities of each mode, highlighted in section 4.2, Juno's AOCS is rather complex. It is based on the simple concept of a spin-stabilized spacecraft, but it's aggravated by the pointing requirements, the expected harsh environment and the required reliability for the mission. The choice for this particular design is due to several motivations: the possibility to grant visibility to multiple payloads with just one mode, the reduction of total mass and complexity and good stability for limited power consumption by exploiting the mass distribution due to the radial positioning of the large solar arrays. The on-board hardware and the rationale behind its choice are here presented.

4.3.1 Sensors

Juno's AOCS employs the following main attitude sensors:

- **2 Stellar Reference Units (SRUs)** custom built by Selex Galileo (now Leonardo S.p.A.) mounted on the forward deck of the spacecraft facing radially outwards. These units are based on the A-STR^[7], modified with further radiation shielding to survive the harsh environment of Jupiter, bringing the total weight of each one up to 7.8 kg.^[8] One of the most important characteristics of these sensors is the ability to operate in a Time Delay Integration (TDI) mode, which allows them to compensate for the spin of the spacecraft when capturing an image. Main specifications of the standard A-STR are reported in Table 4.2.

FOV [deg]	Bias Error [arcsec]	FOV error [arcsec]	Mass [kg]	PC [W]	OT [°C]
16.4 × 16.4	8.25 (pitch/yaw) 11.1 (roll)	< 3.6 (pitch/yaw) < 21 (roll)	3.55	8.9 @ 20°C 13.5 @ 60°C	-30 to +60

Table 4.2: A-STR specifications

- **2 Spinning Sun Sensors (SSSes)** by Adcole Maryland Aerospace^[9], positioned on the edge of the forward deck oriented in such a way to include both the Z-axis and a portion of the XY plane in their FOV. They are specialized in attitude determination on a spinning spacecraft and allow for a fail safe recovery. Useful specifications are shown in Table 4.3.

FOV [deg]	Accuracy [deg]	Mass of sensor [kg]	Mass of electronics [kg]	PC [W]
± 64	± 0.1 at 0° ± 0.6 at 64°	0.109	0.475 to 0.725	0.4

Table 4.3: SSSes specifications

- **2 Inertial Measurement Units (IMUs)** by Northrop (hypothesizing heritage from Cassini^[10] and MESSENGER^[11]) placed inside Juno's radiation vault. One of their biggest advantage is utilizing Hemispherical Resonator Gyroscopes (HGRs) which, due to their construction and inner workings, are inherently radiation hardened and highly resistant to wear and ageing. In particular, SSIRUs^[12] are used, also modified for this specific mission like the A-STR. Their nominal specifications are shown in Table 4.4.

Power [W]	Weight [kg]	OT [°C]	ARW [deg/√hr]	HAMRR [deg/s]
43 max	7.1	-55 to +85 (non-operational) -10 to +60 (full performance)	< 0.00015	± 7

Table 4.4: SSIRUs specifications

All of these sensors are doubled to provide cold redundancy, meaning that only one unit is powered during nominal operations while the other one is switched off. An additional sensor suite, the **Advanced Stellar Compass (ASC)**, is present on Juno to support the MAG experiment. It's comprised of four **Camera Head Units (CHUs)**, two per each FGM for redundancy, mounted on the MAG boom pointing towards the -Z direction and inclined by ± 13° along the Y-axis. Their objective is to achieve a more precise attitude determination near the instrument location with the help of the SRUs, which can also function as a backup in case the ASC fails. These sensors were designed and built by the Technical University of Denmark (DTU) as largely off-the-shelf products.^[13]

4.3.2 Actuators

As previously described in the analysis of the propulsion system (Homework 2), Juno utilizes twelve MR-111C RCS thrusters by Aerojet Rocketdyne^[14] divided into four redundant groups of three. Each set is housed on a Rocket Engine Module (REM) on top of four pylons, two on the forward deck and two on the aft deck, extending in the Z-axis and mounted along the Y-axis. The pylons are raised respectively by 74 cm on the forward deck and about 26 cm on the aft deck. As shown in Figure 4.5, each cluster includes an axial thruster, denoted by the letter "A", and two lateral ones, denoted as "L". Axial thrusters are canted 10° away from the Z-axis while the lateral thrusters are canted 5° away from the X-axis and 12.5° toward the Z-axis^[5]. The specifics of the MR-111C thrusters are presented in Table 4.5.^[15]

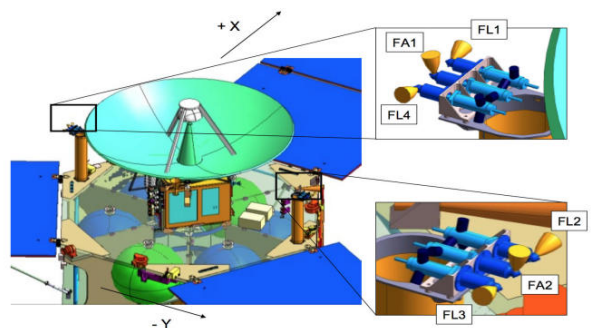


Figure 4.5: RCS mount direction

Thrust [N]	I_s [s]	MIB [Ns]	Propellant	Catalyst	Mass [kg]	Power usage [W]
4.5	220	0.08	Hydrazine	S-405	0.33	13.64

Table 4.5: MR-111C specifications

Additional hardware is present on the spacecraft to aid attitude control, while not being full-fledged actuators. In particular the supporting struts of the three solar arrays can be moved to adjust their position in order to align the principal inertia axis with the geometrical Z-axis.^[16] An active nutation damper is also installed on-board, able to reduce unwanted nutation by generating a controlled damping torque.^[17] Given the stringent pointing requirements an active system was chosen for its higher damping rate with respect to a passive one.

4.3.3 Rationale

Like all other subsystems of the spacecraft, the specific AOCS components were mainly chosen for their high TRL and heritage due both to the complexity of the mission and the harsh environment of Jupiter. Further criteria for the selection, positioning and use case of each unit type can be highlighted:

- **SRUs:** star sensors are the most accurate and are capable of complete AD independently of any other sensor. They are used during all modes except for the TBTM and the SM-2, during which they are shut down ([subsection 4.2.5](#)). Magnetometers weren't really taken into consideration due to the lack of an accurate model of Jupiter's magnetic field and the long interplanetary cruise. This leaves sun sensors and IMUs as possible options but neither could be used as the main source of AD due respectively to low accuracy or the necessity to be periodically realigned. SRUs positioning is dictated by the need of leaving their FOV unobstructed.
- **SSSes:** one of them is always on to further enhance AD, while both of them are used during SM-2 to obtain a coarse attitude determination. Since a SM entry could happen at any point of the mission the FOVs of the SSSes need to cover all possible orientations of Juno: Earth pointing, Sun pointing and the pointing for ME burns. Sun sensors were chosen for this task due to their large FOV, simple design and high reliability.
- **IMUs:** sun sensors aren't capable of a complete AD while the SRUs aren't being used, so during TBTM another component able to do so is required and IMUs were the only remaining choice. They are also employed during large precessions (larger than $\sim 2.5^\circ$) and required for active nutation damping and spin control.^[17]
- **RCS Thrusters:** thrusters were chosen since they are able to provide a high control torque while remaining compact and integrated with the propulsion system. On the contrary reaction wheels and CMG would take up much more space to generate the same control action, thus being less space efficient and cumbersome, especially on a spin-stabilized S/C. Magnetorquers weren't even considered as they need magnetometers to be effective, so they have same limitations described above. Regarding the thrusters' positioning, the orientation presented in [subsection 4.3.2](#) is due to the need of limiting the interaction of the exhaust gasses with the on-board instruments, the HGA and the solar arrays. Being the only actuators present on-board, thrusters are used during all control modes.

4.4 Reverse sizing of AOCS

In this section a reverse sizing of the AOCS is performed. The complexity of the dynamics of a spin-stabilized satellite only controlled via RCS required the use of a Simulink model, specifically developed for this assignment and presented in [appendix 4.5.1](#).

4.4.1 Modeling hypothesis

The preliminary reverse sizing process is based on some simplifying assumptions:

- **Geometry:** Juno spacecraft has been modeled via SolidWorks software, simplifying its shapes but conserving the general dimensions, in particular the size of the solar panels, the vault and the central body. The mass of the system is assumed to be constant throughout the whole mission, at 3625 kg, so the propellant mass needed is overestimated. Principal moments of inertia, calculated from the centre of mass, are assumed to be aligned with the geometric axes of the model: this assumption is pretty compliant with the real satellite dynamics thanks to the actuators mounted on solar panel as described in [subsection 4.3.2](#).

The central body was designed as an hexagonal prism with an height of 1.48 m and sides of 1.79 m, the three solar arrays as thin panels of 8 m \times 2.7 m \times 0.03 m, one of them shorter at 6 m due to the presence of the MAG boom, the vault as a rectangular prism of 0.8 m \times 0.8 m \times 0.7 m and the HGA as a rotational ellipsoid with a major semi-axis of 1.25 m and a minor semi-axis of 0.625 m. A view of the CAD model is presented in [Figure 4.6](#).

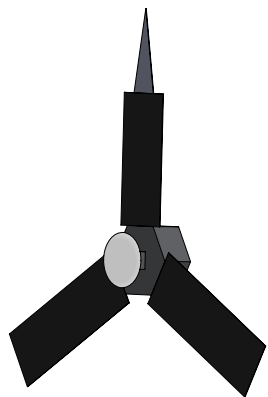


Figure 4.6: Juno CAD model

- **Sensors:** the attitude of the spacecraft is assumed to be correct at all times. No errors are present as nor SRUs nor IMUs nor SSSes were modeled.
 - **Thrusters:** all twelve thrusters are decoupled one from the other. This assumption changes the dynamics of the spacecraft as the real satellite has to perform consecutive burns via RCS in VECM while in the model only one burn is required. Different arms for each thruster were considered as they are not symmetrical with respect to the centre of mass: 2.7 m for thrusters controlling X and Y-axis, 3.2 m for thrusters controlling the Z-axis.
 - **Controller:** the performance of the various manoeuvres is influenced by the chosen control law. Parameters such as maximum angular speed, acceleration and total time of the manoeuvres are checked to verify the obtained results.
 - **Phases:** only two phases have been simulated, each with its own set disturbances: IC from L+3d to L+822d and jovian planetary phase. OC was not considered as SRP lowers and no other significant disturbances act on Juno. However, the same amount of fuel consumed during ICs will be allocated for the OC to point Earth for telecommunications. For the IC phase three different sections are considered: IC 1, IC 2 and IC 3. Relations between these sections and different modes are shown in [Figure 4.4](#). Sun pointing has been considered for all three sections as a worst case scenario sizing, even if IC 2 is in Earth pointing mode (Earth and Sun are almost aligned in this section so the reasoning is not that far off). During each section of the IC, the SRP is considered constant and equal to the integral mean value calculated on the length of the section. For the correction manoeuvres the following scheme was implemented: the spin rate is continuously controlled while the spin axis is realigned every 20 days through a 20 minutes correction manoeuvre. This saves a considerable amount of propellant with respect to an uninterrupted control of both attitude and angular speed while always remaining compliant with the constraints shown in [Table 4.1](#). Slew manoeuvres are also considered to take into account the movement of the spacecraft relative to the Sun as the pointing cannot be considered inertial. The simulation takes into account only one trial and assumes that no differences are present between contiguous sections. Realignments of Juno's axes can be related, in general, to correction manoeuvres as the system is able to handle different disturbances from the nominal orbit.
- Jupiter planetary phase takes into account SRP, magnetic disturbances and gravity gradient (GG). An 11-days elliptical orbit was considered for the simulation and repeated 33 times as required by the nominal mission.
- **Manoeuvres:** two different kinds of manoeuvres were modeled: slew manoeuvres and SCMs. The first ones are executed at each DSM, where the TBTM is employed. A worst case scenario has been identified, within the DSMs requirements, with a change of 90° in angular momentum orientation. Observed rate of this manoeuvre from Nasa Eyes^[18] shows an angular velocity of about 0.1 °/s. This will be used as the maximum value allowed. To simulate SCM only the component along the main spin axis (Z-axis) is controlled and no attitude corrections are performed.

4.4.2 Perturbations

There are four attitude perturbations that need to be analyzed: solar radiation pressure (SRP), gravity gradient (GG), magnetic and aerodynamic disturbances. In the harsh environment of Jupiter some of those have a significant impact on the spacecraft, while others could be neglected.

- **Magnetic Torque:** this disturbance was considered only around Jupiter. The model used to describe its magnetic field consists in a dipole modeled around the work of Acuña et al^[19], and its value is shy of $4.3 \cdot 10^{-4}$ T. Juno's magnetic dipole was assumed from literature, considering a high value of 0.05 Am^2 as a worst case scenario.
- **SRP:** this disturbance is considered both during the IC and the jovian phase. However, in the latter phase it has a less relevant effect as the intensity of the radiation coming from the Sun goes as the inverse of the distance squared. Values considered in the different phases and sections are reported in [Table 4.6](#). As can be seen in the first row of this table, solar radiation is higher during IC 1 and 3, where the spacecraft is closer to the Sun. SRP applies a force on different surfaces: the cross section of Juno that faces the Sun is 70 m^2 . As a first approximation this value was divided in three equal parts, as the number of solar arrays: the torque is computed by considering the SRP acting in the barycenter of each panel. The large area considered made the SRP the dominant perturbation throughout the whole IC phase, despite of the distance from the Sun. The total torque is only applied to the Y-axis due to the geometry of the spacecraft. Reflectivity was assumed as 0.55 for all surfaces facing the Sun, while the arms for the torque were calculated from the CAD model.
- **Gravity Gradient:** this disturbance is considered only during the planetary phase around Jupiter. As can be seen from the last row of [Table 4.6](#), it is orders of magnitude lower than the SRP during the other phases. The torque considered for the various ICs is derived from the average distance between Juno and the Sun, while the value for the jovian phase is reported as the maximum found around the whole orbit. To avoid considering only the worst case, the dynamics of this perturbation was also modeled during a nominal 11-days orbit.

	IC 1	IC 2	IC 3	Jovian phase
$F_s [W/m^2]$	1225	413	1339	$4.08 \cdot 10^{-2}$
$Torque_{SRP} [\text{Nm}]$	0.991	0.33	1.08	0.04
$Torque_{GG} [\text{Nm}]$	$3.5 \cdot 10^{-10}$	$5.4 \cdot 10^{-11}$	$3.5 \cdot 10^{-10}$	$5.39 \cdot 10^{-4}$

Table 4.6: SRP and Gravity Gradient relevant values

- **Atmospheric Drag:** this disturbance is meaningful only in case of a dense atmosphere. During the IC phase Juno is in vacuum, so no atmosphere is present. For the planetary phase, instead, Jupiter's atmosphere needs to be evaluated: at 1000 km of altitude, density is already in the order of 10^{-11} kg/m^3 and Juno's closest approach is above 4000 km. Supposing an exponential decay of the density with altitude (as in Earth's atmospheric model) the value of the density allows to neglect the atmospheric drag^[20].

4.4.3 Propellant reverse sizing

Results of the control action in various scenarios are analyzed in this section.

- **SCM:** this control mode is employed 10 times to change the angular speed of the spacecraft in order to perform both ME burns and science operations. Nominally Juno is spinning at 1 RPM during every cruise phase, 2 RPM during science operations and Fly-by and at 5 RPM during all ME burns. A total of 10 manoeuvres of this kind were performed, 5 spin-ups and 5 spin-downs, distributed along the whole mission. A total of 33.14 kg of hydrazine was found to be consumed. A maximum acceleration of $0.05^\circ/\text{s}^2$ was observed. In Table 4.7 the amount of fuel utilized for each single change in spin is reported together with the number of times it had to be performed, in one way or the other. Spin changes reported in the first column were performed before and after DSMs and before JOI; the ones in the second column were executed before and after the Fly-by; the ones in the last column were done after the JOI and before and after the PRM.

	1 RPM \leftrightarrow 5 RPM	1 RPM \leftrightarrow 2 RPM	2 RPM \leftrightarrow 5 RPM	Total
Fuel Consumption [kg]	4.27	1.07	3.21	33.14
# of occurrences	5	2	3	10

Table 4.7: Spin change manoeuvres

- **Slew manoeuvre:** this specific manoeuvre is performed eight times to align the ME with the required direction to perform a burn (subsection 4.2.5): twice for each DSM while spinning at 1 RPM, twice for the JOI (once spinning at 1 RPM and once spinning at 2 RPM) and twice for the PRM while spinning at 2 RPM. A worst case scenario is always considered with a 90° realignment.^[16] All the slew manoeuvres are performed with a maximum velocity of $0.1^\circ/\text{s}$ as stated in subsection 4.4.1. Given the considerable moment of inertia along the Z-axis, a higher rotational speed implies a significant augment in fuel consumption. Results are of 2.7 kg for each slew at 1 RPM and 6.28 kg for each slew at 2 RPM. Total consumption for these manoeuvres is 32.34 kg.
- **Interplanetary Phase corrections:** in this control mode only the SRP is considered affecting both angular speed and attitude of the spacecraft. Corrections of the angular velocity are continuously performed to ensure stability in pointing without correcting the attitude directly. However, after a 20-days period, corrections are needed to align the HGA to its nominal pointing requirement.^[16] All the constraints cited in subsection 4.2.9 are respected. The consumption of hydrazine in these phases is reported in Table 4.8.

	IC 1	IC 2	IC 3	Total
Fuel Consumption [kg]	4.82	3.00	13.94	21.76

Table 4.8: IC consumption

- **Jovian planetary Phase:** while orbiting Jupiter, Juno performs science spinning at 2 RPM, ensuring natively higher robustness to disturbances. Major corrections must be performed near the pericentre of the orbit, as its speed approaches 58 km/s. Requirements in pointing have been satisfied in this phase as the maximum error achieved during the simulation was lower than 0.025° . Consumption of hydrazine is estimated at 1.01 kg per orbit, 33.24 kg for the whole nominal mission. An important note shall be made in regards of the planetary phase: propellant consumption is based on the 11-days orbit around Jupiter, which were never performed. Consumption during the real 53-days orbit is actually lower, as both gravity gradient and magnetic disturbances diminish with distance, allowing for a longer life mission.

A total of 142.24 kg of fuel was found to be consumed by the AOCS. If margins are considered as in Homework 2, considering that no orbital corrections (OTMs and TCMs) were taken into account, the computed value is shy of the real on-board mass.

4.5 Appendix

4.5.1 Simulink model description



Figure 4.7: Simulink model of the dynamics

The model used to mimic the dynamics of Juno is reported in Figure 4.7. Three main blocks can be distinguished:

- **Dynamics and kinematics:** the behavior of the spacecraft is described through Euler equations and the attitude kinematics is continuously updated via Euler angles.
- **Disturbances:** all the disturbances affecting Juno's attitude are here implemented. Based on the different requirements of the phase, only some are considered. For the planetary part, the highly elliptical orbit has been modeled as a restricted two-body problem.
- **Control:** this part is responsible of calculating the target attitude and its error at each time-step, allowing the controller to satisfy the pointing requirements of the current phase.

Bibliography

- [1] Bill Kurth. "Juno Spacecraft Description". In: (2012).
- [2] Stuart K. Stephens. "The Juno Mission to Jupiter: Lessons from Cruise and Plans for Orbital Operations and Science Return". In: (2015).
- [3] Shadan Ardalan et al. "Juno Orbit Determination Experience During First Year at Jupiter". In: (2017).
- [4] M. A. Janssen. "MWR: Microwave Radiometer for the Juno Mission to Jupiter". In: (2017).
- [5] Thomas A. Pavlak et al. *Maneuver Design for the Juno Mission: Inner Cruise*. AIAA space forum. Site: <https://arc.aiaa.org/>. 2018.
- [6] Anthony P. Mittskus et al. "Juno Telecommunications". In: (2012).
- [7] Leonardo S.p.A. *AUTONOMOUS STAR TRACKERS*. Site: https://space.leonardo.com/documents/16277711/19573187/Copia_di_A_STR_Autonomous_Star_Trackers_LQ_mm07786_.pdf?t=1538987562062.
- [8] H. N. Becker et al. "The Juno Radiation Monitoring (RM) Investigation". In: (2017).
- [9] Adcole Maryland Aerospace. *Fine Spinning Sun Sensor*. Site: https://satcatalog.s3.amazonaws.com/components/362/SatCatalog_-_Adcole_Maryland_Aerospace_-_Fine_Spinning_Sun_Sensor_-_Datasheet.pdf?lastmod=20210708050522.
- [10] Sergei A. Jerebets. "Gyro Evaluation for the Mission to Jupiter". In: (2007).
- [11] Daniel J. O'Shaughnessy et al. "MESSENGER IMU INTERFACE TIMING ISSUES AND IN-FLIGHT CALIBRATION RESULTS". In: (2006).
- [12] Northrop Grumman. *Scalable SIRU™ Family*. Site: <https://cdn.northropgrumman.com/-/media/wp-content/uploads/pdf/Scalable-SIRU-family-of-products-brochure.pdf?rev=57f1ba8ddcb44783b9e97f979b6e45d9>.
- [13] Patricia Lawton Jack Connerney. "Juno Magnetometer (MAG) Standard Product Data Record and Archive Volume Software Interface Specification". In: (2018).
- [14] Aerojet Rocketdyne *Propulsion plays role in Juno mission*. Online Communication. Site: <https://www.proquest.com>. 2016.
- [15] *MR-111C datasheet*. Site: <http://www.astronautix.com/m/mr-111.html>.
- [16] Jeff Lewis. "Juno Spacecraft Operations Lessons Learned for Early Cruise Mission Phases". In: (2014).
- [17] Site: https://pds.nasa.gov/ds-view/pds/viewContext.jsp?identifier=urn:nasa:pds:context:instrument_host:spacecraft.jno.
- [18] *Eyes on the solar System*. Site: <https://eyes.nasa.gov>.
- [19] Mario H. Acuña et al. "Physics of the Jovian magnetosphere". In: (1983).
- [20] Cianciolo et al. "Jupiter Global Reference Atmospheric Model (Jupiter-GRAM): User Guide". In: (2021).

Homework 5

Notation

TCS	Thermal Control System	MLI	Multi Layer Insulation
C&DH	Command Data Handling	SPM	Sun Pointing Mode
IMU	Inertial Measurement Unit	EPM	Earth Pointing Mode
SRU	Stellar Reference Unit	HGA	High Gain Antenna
SSS	Spinning Sun Sensor	LILT	Low Intensity and Low Temperature
MWR	Microwave Radiometer	SOI	Sphere Of Influence
JEDI	Jupiter Energetic-particle Detector Instrument	JOI	Jupiter Orbit Insertion
JADE	Jovian Auroral Distribution Experiment	EGA	Earth Gravity Assist
UVS	Ultraviolet Spectrograph	EOM	End of the Mission
JIRAM	Juno Infra-Red Auroral Mapper	IR	InfraRed
MAG	Magnetometer	ME	Main Engine
MOB	Magnetometer Optical Bench	RCS	Reaction Control System
FGM	FluxGate Magnetometer	q_{sun}	Solar heat flux [W/m ²]
CCD	Charge Coupled Device	q_{tot}	Total heat flux [W/m ²]
CHU	Camera Head Unit	Q_{in}	Internal generated heat [W]
SP	Solar Panels	Q_{ht}	Heater power [W]
KaTS	Ka-band Translator	Q_{lv}	Heat dissipated by the louvres [W]
TWTA	Traveling Wave Tube Amplifier	α	Absorptivity [-]
SDST	Small Deep Space Transponder	ϵ	Emissivity [-]
TP	Thermal Phase	σ	Stefan-Boltzmann constant [W/m ² K]
LEOP	Launch and Early Orbit Phase	T	Temperature [K]
IC	Inner Cruise	A_{tot}	Total area of equivalent sphere [m ²]
OC	Outer Cruise	A_c	Cross section area of equivalent sphere [m ²]
DS	Deep Space	A_{sp}	Solar panels area [m ²]
S/C	SpaceCraft	$(\cdot)_{mb}$	Main body
		$(\cdot)_{sp}$	Solar panels

5.1 Introduction of TCS

The Thermal Control System of Juno adopts various strategies in order to maintain the instrumentation within operative ranges of temperature. This is done through both active and passive systems, which will be analyzed in [section 5.3](#). First thing first, an analysis of the mission will be conducted to enlighten the thermal conditions the satellite is exposed to, which range from really hot environment nearby the Sun to extremely cold environment nearby Jupiter. A selection of the two most extreme situations will be done through a preliminary evaluation of the heat fluxes in these phases. In the light of this, the architecture of the Juno's TCS will be studied and justified through a brief rationale analysis. Finally, a reverse sizing will be carried out imposing some simplifying assumptions in order to find the temperatures on Juno and to verify the compliance with its mission.

5.2 Analysis of thermal conditions along the mission

In this section, the mission will be analyzed and divided in perspective of thermal environment encountered. During this study, the internal heat flux generated by instrumentation won't enter the reasoning. This is done because its maximum value and its variability are both contained during the mission, so it won't affect the sectioning of the TPs and the selection of the hot and the cold cases. The architecture of the S/C won't affect the reasoning and only the heat fluxes from the external environment (Sun flux, planets' albedo and IR emission) will enter this preliminary analysis. A deeper study will be conducted during the reverse sizing in [section 5.4](#).

5.2.1 Thermal phases analysis

Different thermal conditions have been encountered by Juno during its cruise. In previous chapters, the mission was divided into phases by different attitude and communication constraints. These phases will be now grouped by the means of thermal constraints to better analyze their evolution during the mission time.

- **TP-1:** in this first phase, which comprehends both LEOP and IC-1, the S/C is in SPM due to thermal and power requirements. In particular, since the trajectory is relatively close to the Sun, Juno has to protect the vault with the HGA (as already explained in the previous chapters). Even if TP-1 is considered a hot phase, it is not the most critical as other phases have more stringent requirements, facing longer periods closer to external heat sources (i.e. Sun and Earth).
- **TP-2:** this second phase corresponds to IC-2. Among the ICs it is the longest and the only one featuring EPM. It does not call for any particular thermal requirement, being Juno farther from both Sun and Earth. No specific attitude is required to thermally control the S/C during the different manoeuvres performed during IC-2. Neither hot nor cold phase is considered along TP-2.
- **TP-3:** the third thermal phase consists of IC-3 till the EGA, performed in SPM to protect the electronics inside the vault as the S/C passes through the perihelion of the orbit (at 0.88 AU). During TP-3, Juno was found to face the most relevant hot environment, occurring at the closest approach to the Sun. As a consequence, this condition was selected to be the hot case.
- **TP-4:** the fourth phase analyzed consists only of the EGA, from the entrance till the exit of Juno from Earth's SOI. This phase contains both a possible hot case and a possible cold case, the first due to the proximity to the planet, the latter due to the eclipse. As a consequence, this is the phase when Juno faces the highest flux excursion of the entire mission. It was found that both of the two conditions are the most extreme in terms of heat flux as the obtained results are linked with the simplified model used. As explained in [subsection 5.2.2](#), these conditions won't be selected as hot or cold case.
- **TP-5:** this phase is the continuation of the TP-3, except that the S/C does not encounter such high flux environment as at perihelion. It goes from the end of EGA till the end of IC-3.
- **TP-6:** this phase only includes the OC up to JOI. The S/C encounters a progressively colder environment as it is going away from the Sun. However, knowing its trajectory, Juno will face colder contexts along its mission. The transition between TP-6 and TP-7 can be seen in [Figure 5.2](#).
- **TP-7:** the last phase goes from the JOI till the end of the mission, including all the science orbits around Jupiter. During this period of time, the spacecraft is subject to the harsh environment of Jupiter, where it faces oscillating flux from the planet: higher nearby the perijoves and lower at the apojoves. Overall, the environment stays cold during the whole phase with a minimum when both Jupiter and Juno are around the apocentre of their respective orbits. This condition is elected as the coldest case of the entire mission.

5.2.2 External heat flux analysis

In order to find the hot and the cold cases, a simplified model of the main external heat fluxes has been carried out. All the formulas for this analysis are reported in [section 5.4](#). To facilitate the computation, some assumptions have been adopted:

- as previously mentioned, only the external heat fluxes have been modeled discarding the internal contribution, which is better treated in section 5.4;
- the only contribution considered during the interplanetary phases is the Sun flux, while in proximity of the planets also albedo and IR emissions are added;
- for the hot case only TP-3 and TP-4 have been analyzed, since the other phases do not have critical condition in this sense;
- for the cold case TP-4, TP-6 and TP-7 have been analyzed, the first because of the criticality of the eclipse condition, the second because of the increasingly farther position of the S/C with respect to the Sun in an interplanetary environment, the third because Juno is orbiting Jupiter at its farthest points from the Sun;
- the analysis has been carried out from the ephemeris of the real mission instead of taking the nominal cruise;
- the $\cos \theta$ factor in the albedo formula is assumed to be always equal to 1 as a conservative simplification, so only the distances are taken into account during the calculations.

The external heat fluxes computed by this simplified model for TP-3 (Figure 5.1), last year of TP-6 and whole TP-7 (Figure 5.2) and TP-4 (Figure 5.3) are shown in the plots below.



Figure 5.1: Flux analysis of TP-3



Figure 5.2: Flux analysis of end of TP-6 and whole TP-7

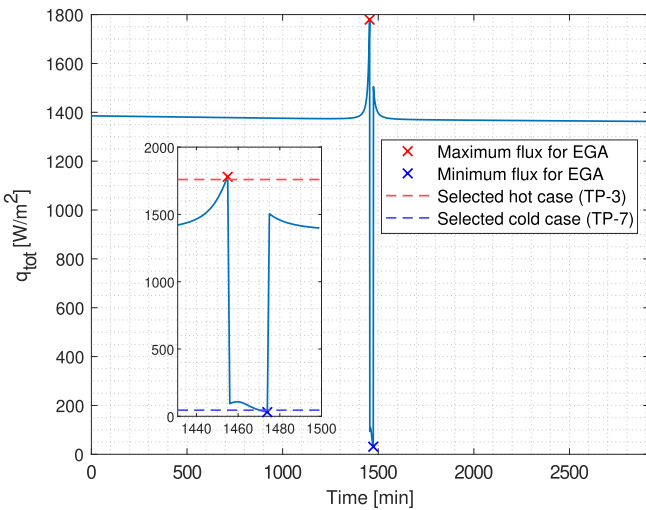


Figure 5.3: Flux analysis of TP-4 (EGA phase)

Phase	q_{tot} [W/m²]
TP-4 hot case	1779.32
TP-3 hot case	1759.23
TP-4 cold case	31.13
TP-7 cold case	45.62

Table 5.1: Summary of considered hot and cold cases

It is worth noting that the flux derived from both planets' albedo contribution is greatly overestimated due to the simplification discussed before. Despite TP-4 presents both the hottest and the coldest points of the whole mission, the time spent by Juno in these regions is limited. As can be noticed in Figure 5.3, the S/C spends only around half a minute in an environment characterized by a heat flux above the one of the hot case (TP-3) and spends around four minutes in an environment where the heat flux is below the one of the cold case (TP-7). Moreover, as can be also seen in Table 5.1, the cases are very close to each other. For this reason, the choice is to not consider EGA's peaks as hot and cold cases, also because in reality Juno has to overcome a transient before reaching extreme temperatures.

The passage from perihelion during TP-3 is hence selected to be the most significant hot environment. On the other side, the most relevant cold case was found to be a few orbits after JOI, around the farthest position of Juno from both Sun and Jupiter, where both solar flux and the planet's contribution are at their lowest. Particularly, in Figure 5.2 oscillations with two different frequencies can be observed: the long period one is related to Jupiter's lightly elliptical orbit around the Sun, the short term oscillation, with its peaks, is related to Juno's highly elliptical orbit around Jupiter. The chosen resolution for the ephemeris determines the non-uniformity of the observed peaks.

5.3 Architecture and rationale of TCS

The TCS of Juno must tackle a wide range of thermal environments, as discussed in section 5.1. The cold case however is the most critical condition for the S/C, so TCS is mainly designed on this situation: the vault, the main body and the external hardware are all thermally insulated and decoupled. Heaters are also present on each individual section/sensor. This guarantees flexibility in order to ensure the operating temperature for each component. Four main thermal zones were identified on the basis of the different thermal requirements of the components and their positioning.

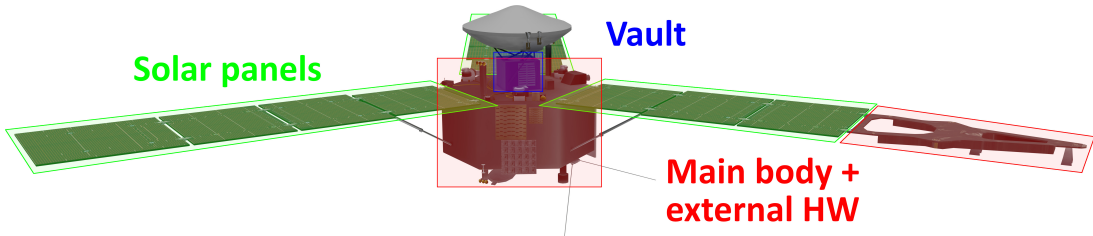


Figure 5.4: Thermal subdivision of Juno

5.3.1 Vault

All the main electronic hardware is contained inside the vault. The size of this box is $0.8 \text{ m} \times 0.8 \text{ m} \times 0.7 \text{ m}$. The lower surface is attached to the main body while the top surface is linked to the HGA, lateral surfaces points outwards and mainly to deep space. The walls are made of 1 cm thick titanium walls^[1]. This metal has a low conductivity value ($\approx 6.7 \div 7.4 \text{ W/mK}$) which is a positive feature for the cold case at Jupiter. Also, major heat generation happens during science orbits since all the instrument electronics is powered on. In addition, the low external thermal flux during science imposes additional requirements in relation to the optical properties of the lateral vault surfaces. Tantalum MLI blankets were used in order to ensure both low emissivity and absorptivity ($\epsilon \approx 0.01 \div 0.035$ ^[2]). However, during the phases in which the thermal flux is at its highest (TP-3), the vault shall be able to dissipate enough power. This is in contrast with the above mentioned design choices. To ensure compatible thermal environment in the vault, three louvres were applied on its external lateral surfaces in order to point deep space and have an efficient IR emission. The dimension of a single louvre is $0.53 \text{ m} \times 0.40 \text{ m}$, two of them are placed vertically while one of them is placed horizontally. The motivation for this choice is relative to the internal configuration of the electronics. The opening of the louvre' shutters raises the emissivity value from 0.14 to 0.74 , enabling higher out-going radiative heat flux.^[3] The justification for this passive and low complexity solution was mainly due to the fact that the hot case scenario was encountered only during a restricted time of the overall mission. Moreover, the louvre technology effectiveness was tested and ensured by previous interplanetary mission such as Rosetta and New Horizons. However, most of the radiation coming from the Sun was shielded by the HGA which protected the vault. The Germanium coated Kapton used to cover the antenna dish has an operating range temperature of $-200^\circ\text{C} \div +200^\circ\text{C}$, while its absorptivity and emissivity values are $\alpha = 0.568$ and $\epsilon = 0.72$ respectively^[4]. The HGA will heat up and exchange radiative heat with the lower vault, hence the necessity to dissipate heat also from the electronic vault with louvres. The electronics contained in the vault are tightly packed to reduce the effects of internal reflection of high energy particles that can still penetrate the walls. From a thermal viewpoint this means that the generated heat is better retained and the internal temperature of the hardware is fairly uniform.

5.3.2 Main body

The main body is the hexagonal prism that contains most of the propulsion subsystem hardware (propellant and pressurizer tanks, feeding lines and ME). Two payload sensors are also present inside, namely UVS and JunoCam. All of these elements require separated strategies to manage the temperatures.

The six spherical propellant tanks (two of oxidizer and four of fuel) are arranged into six bays that corresponds to the equally distributed volumes of the the hexagonal prism. Hence, each compartment contains just one tank and it is thermally uncoupled from the others in order to guarantee a better independent and redundant thermal management. To ensure this uncoupling, high reflectance blankets are used over the tank surface. Nominally, aluminized polyester film is used ($\alpha/\epsilon \approx 3.5$). This material minimizes heat flow to and from the S/C, it is generally

used for temperature ranges from -250 °C to +120 °C and has been successfully used on previous missions^[5]. The tanks are made of titanium which has low thermal conductivity. The honeycomb composite lateral walls of each bay are also covered with high reflectance coating to ensure radiative insulation. In addition, heaters are present into the propellant tanks, helium tanks and also feeding lines.^[6] Other thermal considerations on the internal main body refers to the operations of the main engine which is mainly inside the central body. In that moments high thermal flux must be handled by the internal structure which must be thermally decoupled both radiatively and conductively.

5.3.3 Solar panels

Three solar arrays are present on the spacecraft to provide electricity throughout the different phases of the mission. They are connected to the main body through hinges and struts. To guarantee the correct pointing towards the Sun, stiffness was required to avoid deformation during the spin. This was obtained using carbon fiber supports on which all the cells are placed. The configuration allows each panel to have a clear view of both Sun and DS: dissipation of heat occurs from both front and back faces as the view factor between panels and Juno's main body is close to 0. Given the described geometry, solar arrays can be modeled as thermally decoupled from the rest of the S/C.

To ensure the proper functioning in drastically diverse environments, solar panels were designed to withstand a wide range of temperatures, going from the predicted +100 °C of the perihelion to the -140 °C around Jupiter^[7]. Moreover, the whole spacecraft has to survive to radiations up to 10^{15} MeV so a custom made CMG coverglass with coating was employed. Every cell of the panels is thus covered on the front side with a 304 µm, 14.3 mil fused silica equivalent^[7], anti-reflective coating and Indium Tin Oxide, the first to improve performance in a LILT environment, the second to mitigate surface charge buildup^[7]. The rear side shielding of each panel's substrate is shielded with a 30 mils fused silica equivalent of Kapton and Germanium. In order to guarantee the correct amount of electricity during science operations, around 440 W at JOI and 400 W at EOM, the arrays are drastically oversized at any distance below 5.4 AU: at 1 AU 14 kW are produced. During the ICs and OC, more electricity than needed is generated but left on the panels in the form of heat that must be dissipated from both front and back faces. To do so, different kinds of coatings are used: values for emissivity vary from 0.84 to 0.88 for Black Kapton on the back side and from 0.66 to 0.88 for the Kapton between cells and the carbon fiber support on the front side. Coverglass on the front side is transparent to the incoming radiation, but it is able to emit towards the DS with an emissivity ranging from 0.73 to 0.82. All the intervals for the reported coefficients are related to hot and cold case^[7].

5.3.4 External hardware

The external hardware thermal zone comprehends all the remaining payload sensors (JADE, JEDI, Waves, MWR, MAG, JIRAM), SRUs, SSSes, batteries, antennas and RCS. Waves and JIRAM are located on the aft deck which can be thought as a cold side since it points deep space. All this hardware is installed either on the main body or on the edge of the solar arrays, hence the visual coupling of main body and external hardware thermal zones in Figure 5.4. JIRAM does not have a minimum temperature range for its sensor, the maximum operating temperature is 95 K in order to have useful scientific data.^[8] Waves sensing unit is composed of the antenna and the pre-amplifier unit which is thermally coated. Conversely to the sensors on the aft deck^[9], JADE and JEDI have minimum operative temperature so they are located on the surface that is in visibility of the Sun (top deck). Moreover, the 4 sensors of JADE and the sensor of JEDI are not directly shielded by the HGA.^{[10][11]} MWR antennas are positioned on two of the six lateral surfaces of the main body.^[12] No stringent requirements are presented for this hardware. During Juno operative life at Jupiter these sensors will face the planet's surface, hence the incoming radiation: albedo and infrared. MAG payload positioning is much more critical under the thermal point of view. The payload is made of two MOBs, each one of them contains the FGM and two CHUs. The two boards are for redundancy. For mechanical and thermal stability requirements, the two MOBs, made of Carbon Silicon Carbide, are linked to the MAG boom, that is composed by aluminum honeycomb between two carbon sheets. To ensure thermal decoupling from the structure, the joints between the magnetic boom and MOBs are made of titanium. Regarding the sensors, both the FGMs and CHUs are located on the side that is pointing deep space. The FGM sensor is enclosed individually within a multilayer thermal blanket and thermally stabilized at all times by a non-magnetic resistive heater driven by an alternating current, which keep the FGM operating temperature close to 0 °C. The temperature gradient between the FGM unit and the MOB is of 80 °C, to reduce the thermal strains on the joints between these two units are made of three titanium joints. This has a double effect: reduce the rotation induced by the gradient and reduce the thermal coupling due to the low conductivity and smaller area of contact. Conversely, the CHUs run at much lower temperature (-54 °C) and thermal gradient is much lower. Their body is made of titanium, they are thermally conditioned with resistive heaters and enclosed into a MLI blanket.

The SRUs (two for redundancy) are located on the top deck, so they receive solar flux while S/C is pointing Earth or Sun. Their hardware is sensible to radiation so the internal components are heavily shielded with tungsten and titanium, the first is thermally conductive while the second is not. Moreover, copper is used as a heat sink to transport thermal energy on the CCD, which is the sensible part of the apparatus.^[13]

RCSs contain also thermal sensible materials, such as the catalytic bed Shell-405, which cannot withstand very cold

environment and it is susceptible to thermal cycles. As a consequence, each set of the three thrusters is heavily shielded and heaters are placed to maintain a minimum temperature.^[14] Most of the external hardware is covered with MLI which guarantees radiative decoupling with low values of emissivity and absorptivity. Moreover, these layers serve as additional protection to the high energy particles radiation of the Jupiter environment.

5.4 Reverse sizing of TCS

The reverse sizing of Juno's TCS focuses independently on the main body and the solar arrays, as they are thermally isolated from each other (subsection 5.3.3). For all analyses only the solar heat flux was considered, as all other fluxes have negligible influence, while the deep space temperature is considered to be 0 K for ease of calculation.

5.4.1 Main body

A first approximate model for the main body consists in a mononodal analysis of an equivalent sphere of the S/C. This sphere has the same area as the exterior of the hexagonal body, radiation vault and HGA combined, for a total of $A_{tot} = 34.78 \text{ m}^2$. The internal generated heat Q_{in} has been recovered from Table 5.6. Its value is reported in Table 5.2 together with the solar heat flux for both cases. From the same Table 5.6 the most stringent operating temperature range was also recovered, ranging from -10 °C to +30 °C.

	$q_{sun} [\text{W/m}^2]$	$Q_{in} [\text{W}]$
Hot case	1759.23	133.48
Cold case	45.62	297.01

Table 5.2: Mononodal analysis solar heat flux and internal heat

Considering now that only the cross section of the sphere is illuminated by the Sun while the whole surface radiates into deep space, the following equation can be recovered by imposing heat equilibrium.

$$\alpha A_c q_{sun} + Q_{in} = \sigma \varepsilon A_{tot} T_{mb}^4 \quad (5.1)$$

This equation can be rewritten to obtain α as a linear function of ε , by fixing all other parameters.

$$\alpha = \frac{\sigma A_{tot} T_{mb}^4}{A_c q_{sun}} \varepsilon - \frac{Q_{in}}{A_c q_{sun}} \quad (5.2)$$

Substituting the extremes of the temperature range for both thermal cases defines two couples of lines in the $\varepsilon - \alpha$ plane. Each pair encompasses a region of plane in which the S/C can operate without any thermal control as seen in Figure 5.5. Their intersection identifies all (ε, α) couples that allow safe operation in both cases.

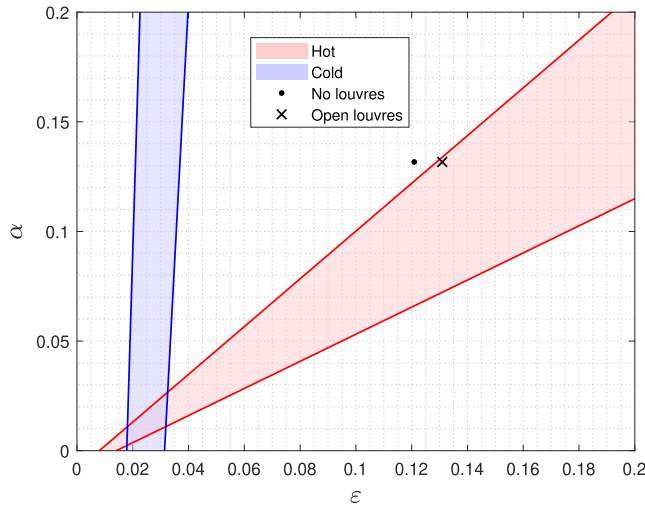


Figure 5.5: Admissible (ε, α) couples

The black dot identifies the specific ε_{mb} and α_{mb} values of the S/C (0.121 and 0.132 respectively), computed as the weighted average of the optical characteristics of the various external surfaces, highlighted in section 5.3, without considering any thermal control hardware. It clearly does not fall into any of the two previously identified regions, meaning that in this model Juno requires both radiators/louvres and heaters to function properly. In fact it's possible

to calculate the S/C temperature from [Equation 5.1](#) imposing all previously defined parameters in both cases. The results are reported in [Table 5.3](#) and, as expected, they are outside the valid range previously identified.

$T_{mb}^{(hot)}$ [°C]	$T_{mb}^{(cold)}$ [°C]
34.91	-77.53

[Table 5.3:](#) Main body temperatures

For both the hot and cold case, then, the minimum heat that needs to be exchanged to keep the temperature inside its range can be computed (Q is positive if heat is entering the S/C):

$$Q_{ht} = \sigma \varepsilon_{mb} A_{tot} T_{min}^4 - \alpha_{mb} A_c q_{sun}^{(cold)} - Q_{in}^{(cold)} = 794.5 \text{ W} \quad (5.3)$$

$$Q_{lv} = \sigma \varepsilon_{mb} A_{tot} T_{max}^4 - \alpha_{mb} A_c q_{sun}^{(hot)} - Q_{in}^{(hot)} = -133.8 \text{ W} \quad (5.4)$$

Where Q_{ht} is the heater power required to keep Juno's main body at the minimum temperature of -10 °C during the cold case and Q_{lv} is the heat that needs to be removed to maintain the temperature at +30 °C in the hot case. The latter can be easily handled by the louvres present on the S/C as can be seen by the position of the black "x" in [Figure 5.5](#), which is inside the hot case viable region. Q_{ht} , instead, is completely unrealistic, especially considering that the solar arrays only produce $\approx 420 \text{ W}$ at Jupiter^[7]. This is caused by the fact that Juno's main body consists of various sections with totally different thermal characteristics and requirements which can't really be lumped all together in a single spherical node model. A multinodal approach that considers both the complex geometry of Juno and the optical properties of each surface independently would yield more realistic conclusions. Furthermore, the results are also in contrast with the cold-biased design of the S/C, where a larger Q_{lv} and a smaller Q_{ht} (in magnitude) would be expected. This is due to the fact that only radiative heat transfer was considered in the model, while neglecting completely the considerable external insulation.

5.4.2 Solar panels

For the solar panels a mononodal analysis was also employed, but in this case the considered geometry is a flat plate with the total area of the solar panels $A_{sp} = 60 \text{ m}^2$. In reality the three arrays are physically separated from each other, but there are no reasons to believe that they will exhibit different thermal behaviors, so they were studied as a single entity. The panels have high absorptivity on the side which points the Sun. This side also points deep space, hence it emits in the infrared. Regarding the back of the solar arrays, the surface only emits in the infrared to deep space. The mathematical modelling is described by the following formula:

$$\alpha_{sp} A_{sp} q_{sun} - Q_{in} = \sigma \varepsilon_{sp} 2 A_{sp} T_{sp}^4 \quad (5.5)$$

Where α_{sp} is the absorptivity of the front surface of the solar array, that is pointing the Sun. Q_{in} is the requested power from all the other hardware of the S/C (without considering heaters), which depends on the mission phase. ε_{sp} is the mean emissivity of the front and back surfaces of the solar array, as both irradiate to deep space, weighted on the area. Since they are equal, it turns out to be just the arithmetic mean. By inverting [Equation 5.5](#):

$$T_{sp} = \sqrt[4]{\frac{\alpha_{sp} A_{sp} q_{sun}}{\sigma \varepsilon_{sp} 2 A_{sp}} - \frac{Q_{in}}{\sigma \varepsilon_{sp} 2 A_{sp}}} \quad (5.6)$$

The known values are the following

α_{sp} [-]	ε_{sp} [-]	A_{sp} [m^2]	$Q_{in}^{(hot)}$ [W]	$Q_{in}^{(cold)}$ [W]	$q_{sun}^{(hot)}$ [W/ m^2]	$q_{sun}^{(cold)}$ [W/ m^2]
0.92	0.825	60	133.48	297.01	1759.23	45.62

[Table 5.4:](#) Input data for solar panels

The temperatures obtained in the two cases are expressed in [Table 5.5](#). Both values are compliant with the specifics of the solar panels given in [Table 5.6](#), so no additional radiators or heaters are needed. These results are also inline with a thermal simulation of the panels performed by NASA itself.^[7]

$T_{sp}^{(hot)}$ [°C]	$T_{sp}^{(cold)}$ [°C]
89.39	-132.11

[Table 5.5:](#) Calculated solar panels temperatures

5.5 Appendix

5.5.1 Thermal limits and power usage of instrumentation

In the following table values for temperature range, power consumption of the different instruments are reported, as well as their respective position.

Instrumentation	Specific element	Temperature range [°C]	Dissipated power [W]	Position
C&DH ^{[15][16]}	-	-55 to +70	2×12	Vault
Tanks & feeding lines ^[14]	-	+10 to +35	-	Main body
Engines ^{[14][17]}	ME	-53 to +65	-	Main body
	RCS	> 0	12×5.39	External
IMU ^[18]	-	-10 to +60	2×43	Vault
SRU ^[19]	Electronics	N/A	2×6.3	Vault
	Optical head	-30 to +60	2×3.7	External
JADE ^[10]	E sensors	-25 to +40	3×0.67	External
	I sensors	-25 to +40	3.8	External
	Electronics	-10 to +45	18.1	Vault
JEDI ^[11]	Sensors	N/A	3×3.1	External
	Electronics	N/A	1.53	Vault
KaTs ^[20]	-	-40 to +65	40	Vault
TWTA ^[21]	-	N/A	2×31	Vault
SDST ^[22]	X/X	-40 to +60	15.8	Vault
	X/X & X/Ka	-40 to +60	19.5	Vault
Batteries ^[23]	-	-20 to +40	-	External
MWR ^[12]	Sensors	N/A	-	External
	Electronics	-15 to +30	32.6	Vault
Waves ^[9]	Sensors	N/A	-	External
	Electronics	-35 to +75	6	Vault
UVS ^[24]	Sensors	N/A	2.5	Main body
	Electronics	-20 to +40	7.3	Vault
JunoCam ^[25]	-	-30 to +75	5.9	Main body
JIRAM ^[8]	-	< -173 ^I	15	External
MAG ^[13]	Sensors	-35 to +75	N/A	External
	Electronics	-40 to +80	N/A	Vault
SP ^[7]	-	-140 to +100	-	External

Table 5.6: Instruments thermal limits and power usage

^I This value only refers to the operational range of temperatures, no limits were found for non operational conditions.

Bibliography

- [1] Installing Juno's radiation vault. *Radiation vault characteristics*. Website. Site: <https://www.nasa.gov/image-article/installing-junos-radiation-vault/>. 2024.
- [2] Robert F. Coker. "Thermal Design and Analysis of Europa Clipper's Radio Frequency Module". In: (2019).
- [3] Sierra Nevada Corporation. *Passive thermal louvers*. 2017.
- [4] A. Carmel Mary Esther et al. "A study on degradation of germanium coating on Kapton used for spacecraft sunshield application". In: (2015).
- [5] Site: <https://www.dunmore.com/products/aluminized-polyester-film.html>.
- [6] Jeff Lewis. "Juno Spacecraft Operations Lessons Learned for Early Cruise Mission Phases". In: (2014).
- [7] William McAlpine et al. "JUNO Photovoltaic Power at Jupiter". In: (2012).
- [8] R.Noschese et al. "JIRAM Standard Product, Data Record and Archive Volume, Software Interface Specification". In: (2013).
- [9] B.T. Mokrzycki et al. "The Juno Waves Investigation". In: (2017).
- [10] D.J. McComas et al. "The Jovian Auroral Distributions Experiment (JADE) on the Juno Mission to Jupiter". In: (2012).
- [11] S.E. Jaskulek et al. "The Jupiter Energetic Particle Detector Instrument (JEDI) Investigation for the Juno Mission". In: (2013).
- [12] M.A. Janssen et al. "MWR: Microwave Radiometer for the Juno Mission to Jupiter". In: (2016).
- [13] R. Schnurr et al. "The Juno Magnetic Field Investigation". In: (2016).
- [14] Nammo. *Leros 1b engine*. Journal of Geophysical Research: Planet. Site: <https://www.nammo.com/wp-content/uploads/2021/03/2021-Nammo-Westcott-Liquid-Engine-LEROS1B.pdf>.
- [15] BAE Systems. *Rad750 experience: The challenge of SEE hardening a high performance commercial processor*. 2002.
- [16] BAE Systems. *RAD750 3U CompactPCI single-board computer*.
- [17] *MR-111C datasheet*. Site: <http://www.astronautix.com/m/mr-111.html>.
- [18] Northrop Grumman. *Scalable SIRU™ Family*. Site: <https://cdn.northropgrumman.com/-/media/wp-content/uploads/pdf/Scalable-SIRU-family-of-products-brochure.pdf?rev=57f1ba8ddcb44783b9e97f979b6e45d9>.
- [19] Leonardo S.p.A. *AUTONOMOUS STAR TRACKERS*. Site: https://space.leonardo.com/documents/16277711/19573187/Copia_di_A_STR_Autonomous_Star_Trackers_LQ_mm07786_.pdf?t=1538987562062.
- [20] S. Ciarcia et al. "MORE AND JUNO KA-BAND TRANSPONDER DESIGN, PERFORMANCE, QUALIFICATION AND IN-FLIGHT VALIDATION". In: (2013).
- [21] Anthony P. Mittskus et al. "Juno Telecommunications". In: (2012).
- [22] General Dynamics. *Small Deep-Space Transponder (SDST)*. 2019.
- [23] Eaglepicher technologies. *Proven battery technology utilizing high energy, long-cycle life, low weight and small volume lithium-ion cells*. 2022.
- [24] G. Randall Gladstone et al. "The Ultraviolet Spectrograph on NASA's Juno Mission". In: (2013).
- [25] C.J. Hansen et al. "Junocam: Juno's Outreach Camera". In: (2013).